THESIS

EVALUATION OF CU-64-ATSM IN CELL CULTURE FOR POTENTIAL USE AS A RADIOTHERAPY AGENT

Submitted by

Dayton Datteri McMillan

Department of Environmental and Radiological Health Sciences

In partial fulfillment of the requirements

For the Degree of Master of Science

Colorado State University

Fort Collins, Colorado

Spring 2014

Master's Committee:

Advisor: Takamitsu Kato

Gerald Callahan
Susan Kraft

ABSTRACT

EVALUATION OF CU-64-ATSM IN CELL CULTURE FOR POTENTIAL USE AS A RADIOTHERAPY AGENT

Oxygen status of tumors is an important clinical factor when considering treatment and potential outcomes. In radiotherapy applications, hypoxic tumors display resistance to traditional low linear energy transfer (LET) external beam radiotherapy (EBRT), instigating interest in finding alternative and more effective means to treat these tumors. ^{64}Cu-diacetyl-bis(N4-methylthiosemicarbazone) (^{64}Cu-ATSM) has shown clinical usefulness in imaging and experimental radiotherapy of solid state tumors due to its ability to concentrate in hypoxic tissue regions and emit radiations of multiple types, energies, and LET. Intrinsic to the potential use of ^{64}Cu-ATSM for radiotherapy purposes is the decay mechanism of ^{64}Cu which emits high LET Auger electrons. Presently, the biological mechanism for cell killing and DNA damage due to high LET electrons released in the decay of ^{64}Cu is unknown. To evaluate how high LET Auger electrons play a role in cell death and DNA damage, Chinese hamster ovary (CHO) cell lines proficient and deficient in DNA non-homologous end joining (NHEJ) DNA repair (10B2 and xrs-5 cells, respectively) were treated with ^{64}Cu-ATSM. Colony formation assay results show similar cell survival for both cell lines treated with similar activities of ^{64}Cu-ATSM, indicating cell lethality due to high LET radiation. Survival curves were compared for radiations of known LET to generally characterize the effective LET of ^{64}Cu-ATSM. Additionally, chromosome aberration and γH2AX DNA double strand break (DSB) studies were performed to examine DNA damage from ^{64}Cu-ATSM. ^{64}Cu-ATSM

was also administered to multiple additional cell lines under various -oxic states to evaluate how efficiently ^{64}Cu-ATSM is incorporated. These findings indicate better ^{64}Cu-ATSM uptake in cancerous, canine, and potentially osteosarcoma cell lines. This research offers experimental support for various characteristics of ^{64}Cu-ATSM that may provide potential clinical advantages over traditional EBRT to more effectively treat hypoxic tumors.

ACKNOWLEDGEMENTS

I would like to thank those on my committee for their help and guidance in the construction of this thesis and willingness to serve as committee members. As the most in depth and central aspect of my degree, having support and help from all of you has been vital to the process. Working with Dr. Kato as my advisor from the start of this project has been a great experience. Taking on responsibility in many phases of this work has been challenging and stressful but has provided a tremendous perspective on creating and carrying out a research project from the ground up which I truly appreciate. I'd like to thank Dr. Furukawa, Dr. Fujibayashi, and the National Institute or Radiological Science (NIRS) for support initiating the work done at Colorado State University (CSU). To those involved in additional aspects of this work including Dr. Kraft, Liz, Jeff, Billie and others at the Veterinary Teaching Hospital (VTH) as well as Jim, Joe, Christy, and Ronda in the Radiation Control Office (RCO) your help was greatly valued.

Completing this project directly involved help from a number of people in the Kato group. Thanks to Justin Bell for consenting to spend long nights in the lab with me doing experiments and Junko Maeda for maintaining and preparing unruly numbers of cell cultures. Thanks to Garrett Phoonswadi for his assistance in imaging the γH2AX experiments. Conversations with Drs. Nagasawa and Genik over the last few years, whether related to research or just for some distraction and storytelling, were always welcome.

Thanks to those at the NIRS and the University of Pennsylvania for the experiences you have provided me in radiation research. Going out and seeing how science and medical research is performed by passionate people at leading institutions

provided perspective and motivation for my education and career that is of the utmost value.

Lastly I'd like to thank those in the health physics section of the department. From my sophomore year when I walked into Dr. Johnson's office I've received so much support and assistance in pursuing my academic interests. After starting out studying agricultural radiological emergency response and eventually moving into applications in biomedical radiation research, feedback from Drs. Johnson and Brandl was always to pursue my interests (even if they weren't 'traditional' health physics). Thanks to department staff such as Julie, Jeanne, Chris, and Erin for their help in navigating my academic pathway. I appreciate all the time and effort spent with my classmates in the health physics program. Funding received from the Nuclear Regulatory Commission (NRC) and Uranium One Inc. has been greatly appreciated as support for my education.

TABLE OF CONTENTS

ABSTRACT ii

ACKNOWLEGMENTS iv

LIST OF TABLES viii

LIST OF FIGURES ix

LIST OF SYMBOLS & UNITS xi

INTRODUCTION 1

Hypoxia 1

Radiation & LET 3

^{64}Cu 7

ATSM 12

CHO DNA Repair Variants 14

Radiation Sources 17

Research Hypothesis & Objectives 18

MATERIALS & METHODS 20

Cell Culture 20

^{64}Cu-ATSM Radiolabeling 21

Colony Formation Assay 23

γH2AX Foci Formation Assay 24

Chromosomal Aberration Assay 25

^{64}Cu-ATSM Uptake 26

RESULTS 28

Colony Formation Assay 28

γH2AX Foci Formation Assay 29

Chromosomal Aberration Assay 31

^{64}Cu-ATSM Uptake 34

DISCUSSION 37

Colony Formation Assay 37

γH2AX Foci Formation Assay 39

Chromosomal Aberration Assay 40

^{64}Cu-ATSM Uptake 42

Future Directions 43

CONCLUSIONS 45

REFERENCES 46

APPENDIX A: RADIOLABELING PROTOCOL 55

LIST OF ABBREVIATIONS 58

LIST OF TABLES

Table 1: Radiations Emitted by ^{64}Cu Decay 8

Table 2: Standard Radiations Used..... 18

Table 3: D_{10} Doses and Ratios for Colony Formation Assay 29

Table 4: 10B2 Chromosomal Aberrations 33

Table 5: xrs-5 Chromosomal Aberrations..... 34

Table 6: CHO & Human Cell Lines for Uptake 36

Table 7: Canine Cell Lines for Uptake..... 36

LIST OF FIGURES

Figure 1: Radiolysis of Water 4
Figure 2: Definition of Linear Energy Transfer (LET) 5
Figure 3: LET Schematic 6
Figure 4: Increased LET of Low Energy Electrons 7
Figure 5: ^{64}Cu Decay Scheme 8
Figure 6: Electron Capture (EC) Process 8
Figure 7: Auger Electron Emission 9
Figure 8: Positron Emission 10
Figure 9: Positron Emission Tomography (PET) 11
Figure 10: Canine CT, PET, and PET/CT ^{64}Cu-ATSM Images 11
Figure 11: Beta Emission 12
Figure 12: Cu-ATSM Structure 13
Figure 13: Ku-80 in Non-Homologous End Joining 15
Figure 14: Hypoxia Gas Composition Dynamics 21
Figure 15: ^{64}Cu Production 22
Figure 16: Cell Survival Fitting Equations 24
Figure 17: Liquid Scintillation Counting Schematic 26
Figure 18: Survival Curves for Cells Exposed to Standard Radiations 28
Figure 19: Survival Curves for ^{64}Cu-ATSM 29
Figure 20: γH2AX Foci Activity Response 30
Figure 21: 10B2 γH2AX Images 31
Figure 22: xrs-5 γH2AX Images 31

Figure 23: 10B2 Chromosomal Aberration Images 32

Figure 24: xrs-5 Chromosomal Aberration Images..... 33

Figure 25: ^{64}Cu Uptake in Various Cell Lines and Conditions 35

LIST OF SYMBOLS & UNITS

Bq	Becquerel
Ci	Curie
D_{10}	dose required to kill 90% of population
eV	electron volt
Gy	Gray
mmHg	millimeter of mercury
m	meter
pO_2	partial pressure of oxygen

INTRODUCTION

Hypoxia

Numerous prognostic factors have been investigated for their potential to enable more accurate projections of treatment outcome following radiation therapy. While many of these prognostic factors would either be impossible or difficult to alter (age, genetics, tumor grading, etc.), ample focus has been directed towards prognostic factors which can be altered for better treatment outcome [1]. One of the most significant and alterable prognostic factors of tumors which could provide benefit in radiation therapy (in addition to chemotherapy, photodynamic therapy, and immunotherapy) is tumor oxygenation [2-5]. Given that tumor hypoxia has been associated with increased tumor aggressiveness, metastatic potential, and failure of local control, efforts to combat this condition are of great interest [6].

Hypoxia is considered a state of abnormally low oxygen concentration in tissue, which to varying degrees is present in 50-60% of human tumors [4]. A hypoxic state in tumor tissue is traditionally considered to arise either through acute or chronic mechanisms [4]. Transient changes which severely reduce microvasculature blood flow or oxygen content are thought to characterize acute hypoxia [5]. Periods of acute hypoxia can be bounded by periods of normal oxygenation, creating a unique environment where cells are constantly adjusting to changing oxygenation. In contrast, chronic hypoxia is due to oxygen diffusion limitations in tissue and lasts for periods of over four hours [5, 7]. As oxygen diffuses through tissue away from blood vessels both cellular metabolism and volume dilution reduce oxygen concentrations. Hypoxia is thought to set in approx. 70 μm from a blood vessel, with tissue in normoxic conditions

closer to the blood vessel and anoxic states more distant from a blood vessel [8]. Both acute and chronic hypoxia in tumors results from abnormal tumor angiogenesis and blood vessel disorganization.

In addition to factors that cause tumor hypoxia, the degree or severity of hypoxia is also important. For most normal subcutaneous tissues the partial pressure of oxygen (pO_2) has been measured to be approx. 50 mmHg, while the median pO_2 for head-and-neck tumors in one study was approx. 15 mmHg [9]. For many clinical studies, a pO_2 of 10 mmHg is often chosen as a cutoff for describing tumors as hypoxic. For relative comparison, a pO_2 of 3 mmHg is roughly correlated to a concentration of about 0.5% oxygen.

Though hypoxia can be present in normal tissues, its presence in tumors is of importance because it modifies cellular functions, in addition to radiation damage mechanisms to be described later. Hypoxia-inducible factor (HIF-1) is a transcriptional factor activated and stabilized under hypoxia [10]. When stabilized, it promotes transcription of genes related to angiogenesis, cell proliferation, and glucose metabolism related to the Warburg effect [10, 11] .

Because of the crucial role hypoxia plays in enhancing tumor survival and therapy resistance a great deal of research has gone into exploration of methods to oxygenate tumors. Methods for tumor oxygenation include mild heating of tumors (hyperthermia) [12], breathing hyperbaric oxygen [13], and treatment with biochemical agents [14-17], which are also designed to target cellular mechanisms making hypoxic tumors treatment resistant. While many methods of reoxygenating tumor tissue have been investigated, an alternative strategy for overcoming the negative effects of hypoxia

in cancer therapy is using a treatment more effective against hypoxic regions of tumors. For radiotherapy, one option is to change the type of radiation to one better able to damage tissues in low oxygen environments.

Radiation & LET

The benefit of using ionizing radiation (IR) to treat tumors is inherent in its ability to damage DNA of cells where dose is absorbed. This dose can be delivered by various types of radiation and targeted to tumor volumes using various technologies, though the predominant way of delivering radiation dose to tumors currently is with photons in EBRT. These high energy x-rays are produced by accelerating electrons produced by a hot, negatively charged cathode filament towards an anode target constructed of a high atomic number (Z) material, typically tungsten. When the electrons collide with the tungsten target they slow through electromagnetic interactions with the nucleus, bending the path of the electrons causing them to release bremsstrahlung x-rays. Using various shielding devices and dosimetry software, these x-rays can be targeted towards a patient's tumor volume effectively. Modern EBRT radiotherapy can be targeted quite locally to tumor tissue while sparing normal tissue and enables high patient throughput, therefore is the most popular method of treating cancer patients with radiation.

A downside to using traditional EBRT for treating hypoxic tumors compared to well oxygenated tumors is approximately three times more dose is required to achieve the same biological effect [3]. This difference arises because EBRT photons damage tissue mainly via an indirect effect. When photon radiation is absorbed by tissue it can eject electrons in the tissue either though the photoelectric effect or Compton scattering. Though this electron may be ejected from an atom incorporated into DNA, the

probability of this is quite low as DNA makes up a small fraction of a cell's mass and volume. On the other hand, as a cell is composed vastly of water (70-85%) the probability is high that ejected electrons will occur on water molecules [18]. This will result in the radiolysis of water and formation of reactive free radicals (Figure 1). If these free radicals (mainly OH·) form in the vicinity of DNA they will be able to react with DNA and produce free radicals on the DNA (DNA·) [8, 19].

$$H_20 + \text{Radiation} \rightarrow H_20^+ + e^-$$

$$H_20^+ \rightarrow H^+ + OH\cdot$$

$$e^- + H_20 \rightarrow H_20^- \rightarrow H\cdot + OH^-$$

Figure 1: The indirect effect of water radiolysis to create free radicals such as these and various others. Free radicals when reacted with DNA are able to cause DNA damage and strand breaks.

In a cell with low oxygen concentration the free radical created on the DNA may be scavenged more readily by an antioxidant (e.g. vitamin C, vitamin E, NADH) , restoring DNA without persistent damage. An environment with higher, or normal, levels of tissue oxygenation does not allow for this damage to be mitigated [8]. Cellular O_2 is able to react with DNA· to create an unrepairable radical. This indirect process is the dominant form of damage for low LET radiation such as x-rays from EBRT (approx. two-thirds of damage from indirect effect), making EBRT less effective at damaging DNA of hypoxic tumor regions than other types of radiations.

Alternatively, radiation may also damage DNA in a manner less dependent on tissue oxygenation. This occurs via the direct effect of radiation and is predominant for high LET radiation. It occurs, as previously described, by the ionization of atoms in DNA. High LET radiation is able to ionize a great deal of DNA if its path crosses DNA

strands. Although indirect damage also occurs without high LET radiation by ionizing water, the amount of damage caused by the direct effect is proportionally greater for high LET radiation compared to low LET.

In categorizing whether a radiation is determined to be of high LET or low LET it is important to assess the distance over which a form of radiation losses energy. LET is most often defined as the change or loss of energy by a charged particle per change in distance (Figure 2) [20].

$$\mathrm{LET} = \frac{\mathrm{dE\ (keV)}}{\mathrm{dl\ (\mu m)}}$$

Figure 2: LET is defined as the average energy lost by a charged particle per distance. Though this is a general definition, LET is most often described in units of keV/μm.

Because photons are not charged particles, their LET is determined by the LET of the fast secondary electrons they create through photoelectric and Compton scattering interactions. For other types of charged particles, LET generally increases with higher charge, mass, and lower speed. Both higher charge and lower energy of charged particles passing through a material allow for greater electromagnetic interaction with orbital electrons, while higher mass allows for less scattering of the radiation. Based on these characteristics α-particles with high charge, mass, and relatively slow speeds are able to impart large amounts of energy in the material they traverse, while fast electrons impart much less (Figure 3) [21].

A useful phenomenon regarding LET of charged particles occurs when they slow down to very low energies. At higher energies, charged particles have less opportunity to interact with electrons in the medium they are passing through. As these charged particles impart energy and dose in a medium, they lose energy, slow down, and have

more time to interact allowing for greater energy and dose deposition the slower they travel, thus increasing their LET. This phenomenon is described as the Bragg peak for heavy particles (protons and heavier) and has been leveraged for external particle beam radiotherapy applications [22]. Though it would be difficult to utilize this Bragg peak property for fast electrons due to their high degree of scatter, thus making it difficult to control where dose is delivered, low energy electrons do provide the ability to deliver high LET radiation (Figure 4) [23]. This is often done using Auger electrons emitted from certain radionuclides, such as ^{64}Cu.

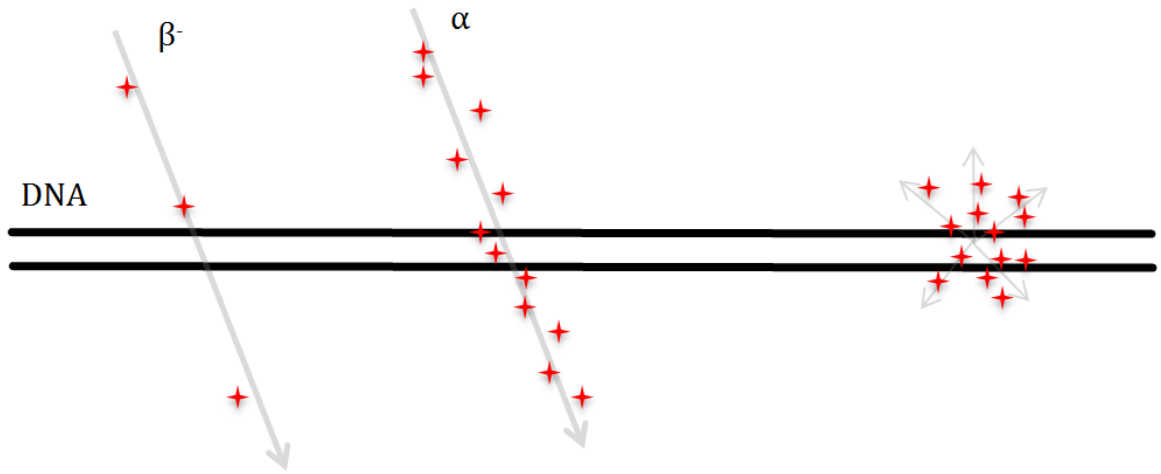

Figure 3: Schematic of different LETs for different forms and energies of radiation. The low energy and localized emission of Auger electrons makes them particularly damaging to DNA if produced nearby.

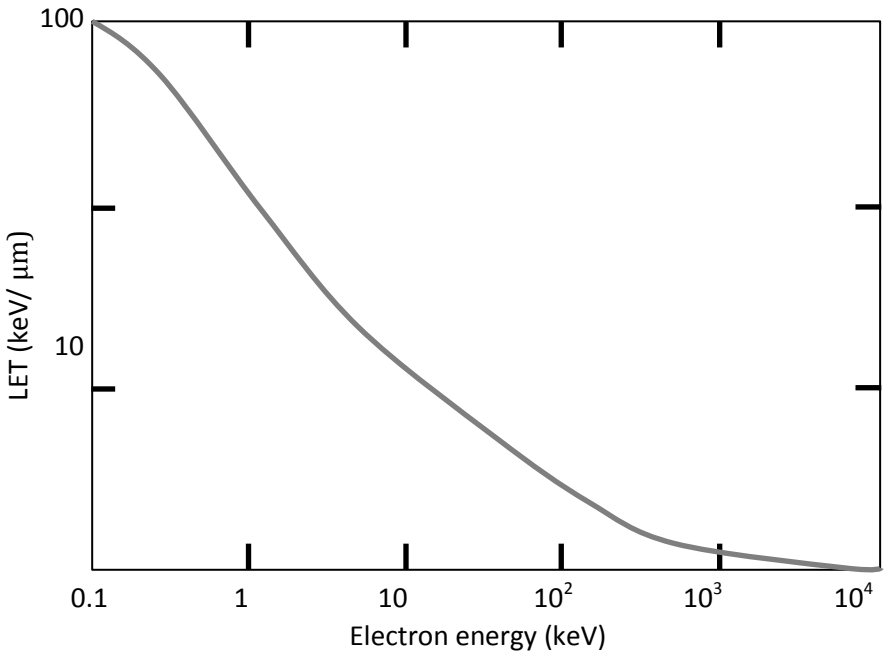

Figure 4: At low energies the LET of electrons increases (Adapted from [24]).

^{64}Cu

Intrinsic to the use of ^{64}Cu in radionuclide therapy of hypoxic tumors is its ability to decay via electron capture (EC) (Figure 5, Table 1). In EC, the proton rich ^{64}Cu nucleus captures an electron from its inner orbital. This electron combines with a proton, creating a neutron and emitting an electron neutrino (Figure 6). Though this decay process and others involve the emission of neutrinos, they have a very low probability of interacting with tissue and are therefore largely irrelevant for radiological health purposes [18]. The resulting electron orbital of the now ^{64}Ni atom is in an excited state since it is missing an inner orbital electron.

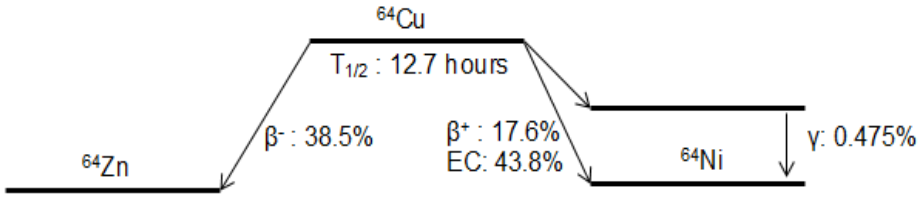

Figure 5: Decay scheme of ^{64}Cu illustrating competition between EC and β^+ decay or β^- decay.

Table 1: Radiations Emitted by ^{64}Cu Decay

Energy Transition	Yield (%)	Energy (keV)	LET (keV/μm)
β^+	17.6	653 (max)	<1
β^-	38.5	579 (max)	<1
γ	0.475	1346	<1
γ (via β^+ annulation)	35.2	511	<1
EC (emits Auger electrons)	43.8	≈0.8-7	≈3-25

$$p^+ + e^- \rightarrow n + \nu_e$$

$$^{64}_{29}\mathrm{Cu} + e^- \rightarrow {}^{64}_{28}\mathrm{Ni} + \nu_e$$

Figure 6: Electron capture (EC) is the process of a proton rich nucleus capturing an electron from its inner electron orbital to gain stability. ^{64}Cu decays by this process 43.8% of the time.

To release energy from its excited state, the atom may either emit characteristic x-rays or Auger electrons. In characteristic x-ray emission, electrons in higher energy orbitals to fall to a lower ground state and the energy difference of the two orbitals are released as x-rays. In Auger electron emission, this energy difference is released as

ejected electrons (Figure 7). As this process ensues more valence states in the electron orbital are created and more and more electrons are ejected. The cumulative process of these ejected Auger electrons is sometimes described as an Auger cascade with about 20 low energy (<10 keV for ^{64}Cu) electrons emitted. The relatively high LET of Auger electrons compared to fast secondary electrons produced by x-rays allow them to damage DNA much more prominently via the oxygen independent direct effect. Originally studied using ^{125}I [25], more work has gone into evaluating many other Auger emitters. Because they are of very low energy, a ^{64}Cu atom would need to decay in the immediate vicinity of DNA (approx. 5 μm, the diameter of a general mammalian cell nucleus) for high LET DNA damage to occur [26].

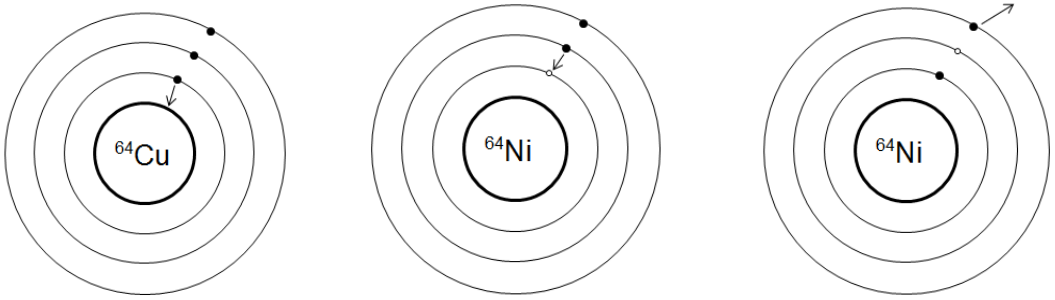

Figure 7: The Auger emission process for ^{64}Cu begins with EC. Higher orbital electrons fall to the vacant lower energy state and transfer excess energy from that transition to another orbital electron, subsequently ejecting that electron and resulting in an additional electron orbital vacancy.

In addition to EC, an alternative decay process to reduce the proton excess of the ^{64}Cu atom is beta plus (positron, β^+, e^+) emission (in addition to a neutrino), an antiparticle to the electron (Figure 8). When the positron is emitted it behaves almost identically to an electron as it travels through material. A difference arises once the

positron loses its kinetic energy. Once it slows to the point it can interact with an electron, the two will annihilate and emit two 511 keV photons in opposite directions. Positron emission requires the decaying ^{64}Cu nucleus to have excess energy of at least twice the mass energy of the emitted positron (1.022 MeV). For ^{64}Cu nuclei there is not always enough excess energy to emit a positron when it seeks stabilization by decreasing its proton number, and in these cases the atom decays through EC.

$$p \rightarrow n + e^{+} + v_e$$

$$^{64}_{29}Cu \rightarrow ^{64}_{28}Ni + e^{+} + v_e$$

Figure 8: Positron decay process which PET imaging is based on.

Radionuclides that decay via positrons are useful for PET imaging [27] (Figure 9). This imaging modality relies upon detection of the 511 keV gammas emitted by a tracer radionuclide injected into a patient. As the tracer radionuclide decays emitting a positron and ultimately two photons, those are emitted from the patient and detected by the surrounding detector system of the PET instrument. Gamma photons interact with a scintillator material and emit light. This light is converted to an electric signal by photomultiplier tubes or other devices. If detectors pick up signals from both annihilation gammas and they can discriminate the time difference between when the signals were registered, the origin of the gammas can be registered along the axis between where the signals were detected. By performing this process for many detected pairs of photons, the three dimensional origin of the photons can be determined. Biological, chemical, or physical markers in the body can be visualized on a PET scan by tagging a tracer radionuclide to specific relevant chemical markers. In cancer imaging, the PET radioisotope can be tagged to molecules specific to metabolic or surface receptors of

cancer cells. By combining a PET scan with a CT (PET/CT) (imaging procedure used to feature anatomy of the body) the anatomical localization of a radiotracer can be obtained three dimensionally (Figure 10).

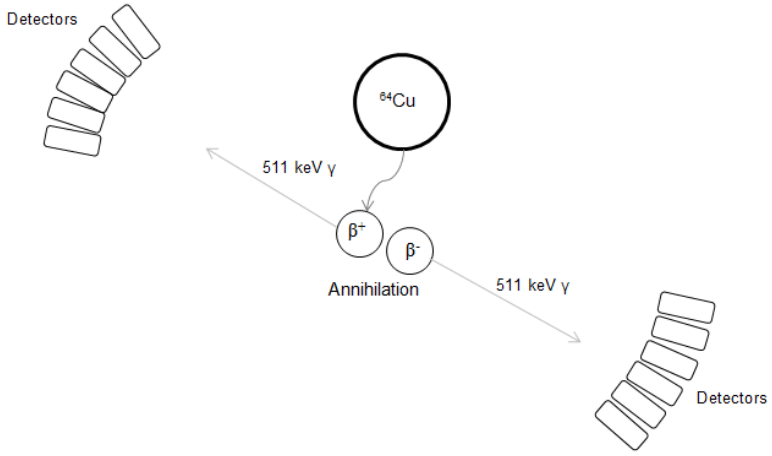

Figure 9: Schematic of the physical and technological process required for PET imaging procedures (Adapted from [28]).

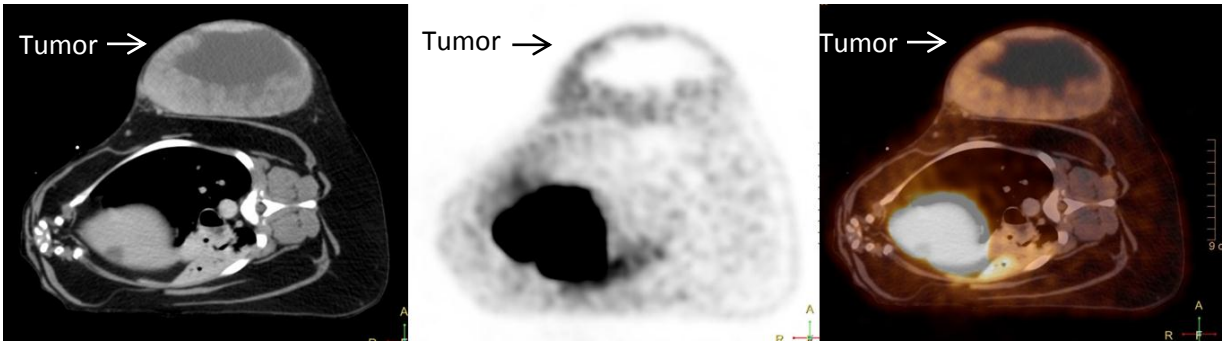

Figure 10: Transverse images of a canine thorax and large chest wall tumor. Canine CT (left), PET (middle), and PET/CT (right) from CSU Veterinary Radiology ^{64}Cu-ATSM imaging study.

While ^{64}Cu can reach a stable state by EC and positron emission to reduce its proton number, it can alternately reach stability by increasing its proton number. This occurs by beta minus (beta, e^-, β^-) emission. In this process a neutron is converted into a proton while an electron and electron antineutrino are ejected from the nucleus (Figure 11).

$$n \rightarrow p^+ + e^- + \bar{\nu}_e$$

$$^{64}_{29}Cu \rightarrow ^{64}_{30}Zn + e^- + \bar{\nu}_e$$

Figure 11: Decay of ^{64}Cu via beta emission.

ATSM

To utilize the decay properties of ^{64}Cu for imaging and potentially radiotherapy applications a suitable carrier agent ATSM has been developed which preferentially localizes to hypoxic tissue (Figure 12). Some important characteristics originally noted about the Cu-ATSM agent which made it potentially useful for imaging purposes were its high permeability across cellular membranes and the ease of copper reduction in hypoxic tissue [29]. This reduction of Cu under hypoxic conditions is thought to allow the copper atom to dissociate from the ATSM agent [30-32]. Though this may occur with some frequency in normoxic conditions, copper may also be reoxidized to allow it to chelate to ATSM once more and potentially diffuse out of the cell or tissue. In hypoxic conditions, this re-chelation likely happens less frequently, allowing Cu to continuously be deposited in hypoxic tissues and cells. Because of these characteristics the agent was considered intriguing for imaging ischemia and hypoxia using positron emitting Cu.

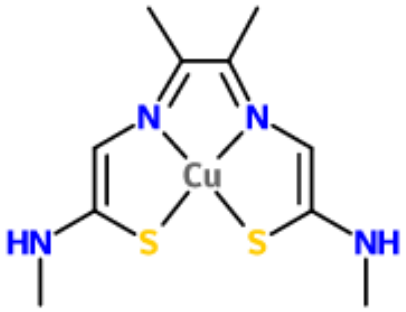

Figure 12: Structure of the Cu-ATSM agent.

Since the initial *in vitro* investigations, studies have shown usefulness of Cu-ATSM in a clinical setting. Its quality as a PET agent is evidenced by its ability to be rapidly deposited in hypoxic tumor regions, with optimal uptake 10 minutes after administration [33], with a high tumor to background tissue ratio which translates to a diagnostic quality PET image acquisition in a clinically practical timeframe [32, 33]. This ability to accumulate in hypoxic tumor tissue has been observed in several cancer lines in a rat model, though some tumor cell lines showed poor Cu-ATSM uptake relative to other hypoxia markers [34].

Also important to consider when contemplating Cu-ATSM agent use in clinical settings is determining the feasibility of creating the agent. All of the copper isotopes studied using ATSM (^{60}Cu, ^{61}Cu, ^{62}Cu, and ^{64}Cu) can be produced on low energy proton cyclotrons [35-37]. As many major regional hospitals and commercial enterprises have these facilities it would be possible to implement production systems. Although this type of cyclotron is available, the installation costs of targeting systems for irradiation of ^{64}Ni and other targets could be a major hindrance in producing copper radioisotopes for large scale distribution. The chemistry to chelate the Cu-ATSM agent is quite simple

relative to other radionuclide agents. Because copper carries only two oxidation states (Cu^{+1} and Cu^{+2}), copper chelation under normoxic conditions and dissociation under hypoxic conditions is a reliable process, making the agent preparation relatively easy.

In addition to animal based studies, Cu-ATSM imaging has been performed on human patients. By imaging patients with cervical cancer prior to treatment with ^{60}Cu-ATSM (pure β^+ emitter) patient tumors could be grossly categorized as hypoxic or normoxic based on the contrast ratio of tumor-to-muscle PET signal [38]. After patients underwent both chemotherapy and radiotherapy and clinical outcomes were evaluated, it was determined that patients with hypoxic tumors as identified by ^{60}Cu-ATSM had significantly worse outcomes than the more oxygenated tumors. Patients also were imaged with the commonly used commercial imaging agent F-18 fluorodeoxyglucose (FDG), and it was determined that FDG signal did not significantly correlate with ^{60}Cu-ATSM uptake, negating any potential use of FDG as a proxy for hypoxia imaging.

While much of the research using Cu-ATSM agents has focused on hypoxia imaging, there has been exploratory work in assessing ^{64}Cu-ATSM as a radiotherapy agent. Preliminary work administering the agent to hamsters with human colon cancer xenographs showed significant increases in survival compared to untreated controls [39]. In this study ^{64}Cu-ATSM was administered in either a single large dose or multiple smaller doses and survival was similar for both treatment regimens.

CHO DNA Repair Variants

To characterize cell death in response to ^{64}Cu-ATSM treatment and determine the effective LET of the ^{64}Cu-ATSM agent, a system of two CHO DNA repair cell lines

was used: normal DNA repair (10B2) and a DNA repair deficient (xrs-5). While the 10B2 line is normal in its NHEJ repair capabilities, the xrs-5 line has a dysfunctional Ku-80 protein involved in recognizing and binding broken DNA ends produced by DSBs in the NHEJ repair mechanism (Figure 13). For higher order eukaryotic cells NHEJ is the major DNA repair mechanism, repairing virtually all DSBs in G0/G1and M cell cycle phases and the vast majority of DSBs in S and G2 phases. Cell killing is considered to result from unrepaired or misrepaired DSBs resulting in inability to separate genetic material equally at metaphase (dicentic chromosomes, acentric chromosome fragments), so an NHEJ mutant such as xrs-5 is sensitive to DSBs caused by IR.

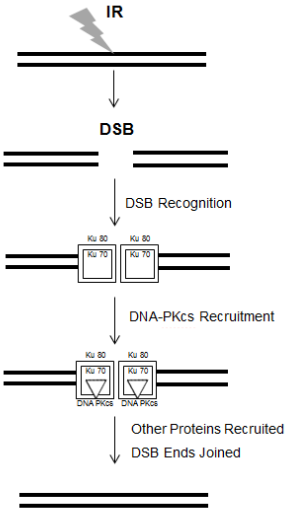

Figure 13: Specific to the cell model used is the DNA repair inefficiency of xrs-5 due to mutant Ku-80 [40]. Ku-80 binds DNA DSBs and serves to recruit other repair proteins in non-homologous end joining (NHEJ).

Mutant Ku-80 protein in xrs-5 is a product of a gene analogous to the human xrcc5 gene [41]. In eukaryotic cells with a functioning NHEJ system, Ku-80 forms a

heterodimer structure with Ku-70 and binds to DNA DSB ends. The bound Ku-70/80 heterodimer recruits DNA-PKcs and activates it as a kinase. Various other proteins are then recruited, and ultimately allow for a functional DNA-PK to form and act joining the ends of a DSB. Without a fully functional Ku-80 in CHO cells, their ability to repair DSBs is greatly reduced. This is significant to the extent that human cells defunct of fully functional Ku-80 are not viable, resulting in embryonic lethality [42].

The ability to determine DNA DSB induction and repair dynamics for these cells is evidenced using the γH2AX foci assay [43]. When DNA DSBs are produced a histone variant, H2AX, near the site is always phosphorylated. This phosphorylation creates the γH2AX form of the histone which plays a role in recruiting proteins to the DSB site which function in DNA repair. When the DNA DSB is repaired its adjacent γH2AX is dephosphorylated to its original form. By utilizing florescent antibodies specific to γH2AX, dynamics of DSB induction and subsequent repair can be observed using florescent microscopy.

The significant differences between 10B2 and xrs-5 cells in their DSB repair capabilities are evident when these cells are irradiated with various LETs of radiation [44]. Mutant xrs-5 cells are less capable of repairing DSBs produced by identical doses of various LETs of radiation, whereas 10B2 cells have improved survival for a given dose of low LET radiation. The reason for this difference is both low and high LET radiation produce the same amount of DNA damage (DSBs and single strand breaks (SSBs)) at a given dose. For high LET radiation, DSBs are produced in DNA closer together, creating more damage in the region of a track, while low LET radiation more evenly distributes DNA damage in the DNA. This concentration of DSBs produced in a

track region by higher LET radiation makes the DNA more difficult to repair and is termed complex DNA damage [45, 46]. The same dose of a lower LET radiation produces less complex or more evenly distributed DNA damage, allowing 10B2 cells to utilize their DNA repair capabilities to more efficiently repair genetic damage and survive.

Based on this concept of similar survival of xrs-5 and variant survival of 10B2 cells to various LETs of radiation, a relative LET of an unknown radiation can be determined. This is important to identify for cells treated with ^{64}Cu-ATSM.

Radiation Sources

Various radiations were used to compile standard survival curves for comparison with ^{64}Cu-ATSM. Radiations ranging from low to high LET were used (Table 2).

Irradiation using a low LET ^{137}Cs (30.17 year half-life) gamma source was performed at Colorado State University (CSU). A second low LET irradiation was performed using a cyclotron accelerated proton source at the National Institute of Radiological Science (NIRS) (Chiba, Japan). A carbon spread out Bragg peak (SOBP) and iron beam at the Heavy Ion Medical Accelerator (HIMAC) at the NIRS were also used. While the proton and iron beams accelerate ions to a single energy, the carbon SOBP accelerates ions to varied energies, or may modulate a single energy beam with varied degrees of shielding. By using different ion beam energies and weighting each individual energy accordingly, an extended depth where the dose or equivalent dose is approximately equal can be created [22]. This extended depth of approximately equal radiation dose is useful in clinical settings.

Table 2: Standard Radiations Used

Source	LET (keV/μm)
^{137}Cs	0.2
Proton	1
Carbon SOBP	≈70
Iron	200

Research Hypothesis & Objectives

Tumors containing hypoxic tissue are significant for their poor clinical outcomes, occurrence in human cancers, and difficulty to treat using various cancer therapy modalities. While many strategies have been pursued to increase tumor oxygenation or modify cellular biochemistry, altering the radiation used to treat hypoxic tumor tissue more effectively is an approach worth further exploration. The ^{64}Cu-ATSM agent provides useful high LET Auger electron radiation and delivers the ^{64}Cu radioisotope preferentially to hypoxic tissue, characteristics descriptive of a radiotherapy agent.

This research seeks to determine whether the effective cell killing action of ^{64}Cu-ATSM is due to high LET Auger electrons useful for hypoxic tumor tissue irradiation.. This was evidenced by evaluating cell survival curves from colony formation assays of ^{64}Cu-ATSM and comparing them to cell survival curves of standard, known LET radiations using two cell lines with unique DNA repair capabilities. Chromosomal aberration and γH2AX foci formation assays were also performed add additional information regarding DNA damage potentially indicative of high LET radiation. Lastly, ^{64}Cu-ATSM uptake experiments were performed using various cell lines under three –oxic conditions with the aim of finding potential candidates ideally suited for either ^{64}Cu-ATSM imaging or radiotherapy applications. We presumed the effective radiation

for cell killing and DNA damage was Auger electrons and expected experimental results to support this assertion. Based on the experimental results, we are be able to consider whether ^{64}Cu-ATSM provides biological evidence for further research and consideration as a radiotherapy agent.

MATERIALS & METHODS

Cell Culture

10B2 cells were graciously supplied by Dr. Joel Bedford (Colorado State University, Fort Collins, CO) and xrs-5 cells were utilized courtesy of Dr. Larry Thompson (Lawrence Livermore National Laboratory, Livermore, CA) [47, 48]. Cell cultures were maintained in a media of Eagle's Minimal Essential Medium Alpha (MEM-α) (Gibco, Indianapolis, IN) augmented with 10% heat deactivated fetal bovine serum (FBS, Sigma, St. Louis, MO), 1% Pen Strep antimicrobial (5,000 U/mL, Gibco), and 0.1% Fungizone antimycotic (Gibco). Cultures were grown and maintained in continual log phase growth by passaging prior to cell confluence. Standard normoxic atmospheric conditions of 5% CO_2 at 37°C were used for cell line maintenance.

Hypoxia was achieved at 37°C by incubating cell culture inside AnaeroPack 2.5L Rectangular Jar (Mitsubishi Gas Chemical Company, Tokyo, Japan) tissue culture boxes (hypoxic chamber) with the addition of one AnaeroPack-Anaero (Mitsubishi Gas Chemical Company) packet inside a 37°C incubator. The AnaeroPack-Anaero sachet serves as an oxygen absorber and CO_2 generator. Per the manufacturer, atmospheric dynamics inside the hypoxic chamber include reduction of the partial pressure of oxygen from approx. 20% to less than 0.1% within about two hours, while CO_2 concentration increases from approx. 0% to 16% or more within an hour (Figure 14). These conditions of hypoxia provide a model for cells transitioning into severe hypoxia, and in this short timeframe would be most similar to that of acute hypoxia onset. Oxygen depletion was verified using RT Anaero-Indicator pills (Mitsubishi Gas Chemical

Company). Anoxic culture conditions at 37°C were reached by injecting N_2 generated by an X-Stream 2000 nitrogen generator (Rigaku, The Woodlands, TX) into a 37°C incubator.

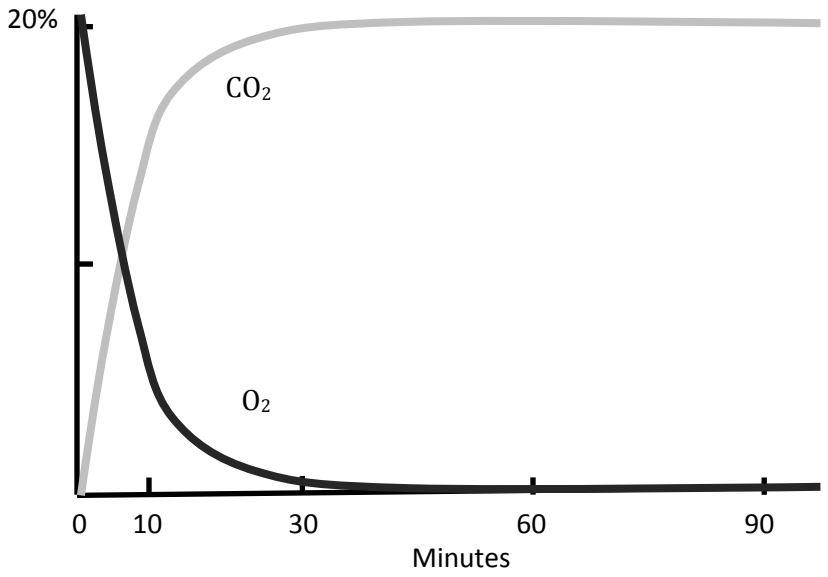

Figure 14: Gas composition dynamics of AnaeroPack-Anaero system used for hypoxia incubation (Adapted from Mitsubishi Gas Chemical Company).

^{64}Cu-ATSM Radiolabeling

^{64}Cu was produced by the University of Wisconsin-Madison Cyclotron Research Group in the Department of Medical Physics by a ^{64}Ni(p,n)^{64}Cu reaction using previously published methods[36] (Figure 15). Shipments of ^{64}Cu in 0.1M HCl solution were received at the nuclear medicine laboratory at the CSU Flint Animal Cancer Center.

$$^{64}_{28}\mathrm{Ni} + \mathrm{p}^{+} \rightarrow {}^{64}_{29}\mathrm{Cu} + \mathrm{n}$$

Figure 15: ^{64}Cu production using proton irradiation of a ^{64}Ni target. As produced by the University of Wisconsin-Madison, 11.4 MeV cyclotron accelerated protons irradiate a ^{64}Ni enriched target.

The ^{64}Cu solution was then checked for its activity using an Atomlab 500 (Biodex, Shirly, NY) dose calibrator. ATSM was provided courtesy of Dr. Takako Furukawa from the NIRS (Chiba, Japan) and synthesized as previously reported [49]. Conjugation of ^{64}Cu-ATSM was performed by first adding equal volumes of ^{64}Cu (in 0.1M HCl) and 4:1:5 1M Glycine, 1N NaOH, and deionized H_20 solution (producing volume A). Next, A volume of 1mM ATSM-dimethyl sulfoxide (DMSO) was added (producing volume B). Finally, B volume of 2% Na-Ascorbate was added and the solution was maintained at room temperature for 20 minutes allowing for Cu-ATSM conjugation. After checking activity, the ^{64}Cu solution was centrifuged and mass was assessed. The solution volume was calculated by subtracting the mass of a tare vial and using the density 0.1M HCl (1g/mL). An equal volume of 4:1:5 1M Glycine, 1N NaOH, and deionized H_20 solution was added to the volume of ^{64}Cu and HCl solution.

Radiolabeling efficiency of ^{64}Cu-ATSM was determined using thin layer chromatography (TLC). A small volume/activity of ^{64}Cu-ATSM solution was added to the bottom of a TLC plate. Using ethyl acetate (Mallinckrodt Baker, Phillipsburg, NJ) as an organic carrier, all bound ^{64}Cu-ATSM was carried in the mobile phase while unbound ^{64}Cu remained in the stationary phase. After the solvent traveled approx. 80% of the TLC plate length the plate was removed from the solvent. Activity on approx. the bottom quarter of the TLC plate was measured in the dose calibrator as that of unbound ^{64}Cu,

while that on the top three-quarters was measured and evaluated as bound ^{64}Cu-ATSM. Radiolabeling efficiency was determined to be 93.1% (s.d. ± 4.7%, n=8). A more detailed radiolabeling protocol is described in Appendix A.

Colony Formation Assay

10B2 and xrs-5 assays were processed similarly for gamma, proton, carbon, and iron irradiations. Gamma irradiation at a dose rate of 2.5 Gy/min was performed at CSU using a Model Mark I-68A (SS0056) 222 TBq (6,000 Ci) ^{137}Cesium sealed source model (J.L. Shepherd, Carlsbad, CA) under standard room conditions. Hadron irradiation was performed using facilities at the NIRS (Chiba, Japan) in standard room conditions. Carbon ions were accelerated to 290 million electron volts per nucleon (MeV/n) and iron ions to 500 MeV/n using the HIMAC synchrotron. Protons were accelerated to 70 MeV/n using the NIRS-930 cyclotron delivery port in C-8. Dose rates for carbon, iron, and protons were set at 1 Gy/min. Cells were asynchronously dividing prior to irradiation. Post irradiation, cells were seeded into 60 mm cell culture dishes (Greiner Bio-One, Monroe, North Carolina) at numbers correlated to expected survival (i.e. more were cells seeded when cells were irradiated with a higher dose). Cells were incubated for seven days in normoxic conditions allowing survivors to replicate. Cells were then washed with 0.9% (w/v) NaCl solution, fixed with 100% ethanol, and stained with 0.1% crystal violet (Wako, Tokyo, Japan). Colonies were counted and those with approx. 50 or more cells were counted as survivors. Doses required for 90% cell kill (D_{10}) were established by fitting survival curves of 10B2 with a linear quadratic function and those of xrs-5 with a linear function (Figure 16). The linear-quadratic function is generally used to model survival for cell cultures exposed to low LET radiations and/or capable of

adequate DSB repair. A linear function is generally used to model cultures exposed to high LET radiation and/or unable to repair DSBs.

$$S = e^{-(\alpha D)}$$

$$S = e^{-(\alpha D + \beta D^2)}$$

Figure 16: The linear (top) and linear-quadratic (bottom) cell survival functions.

For ^{64}Cu-ATSM studies,10B2 and xrs-5 cells were maintained in log phase growth before being plated into T12.5 tissue culture flasks (BD Biosciences, Franklin Lakes, NJ) three hours prior to ^{64}Cu-ATSM experiments to allow adhesion to culture flasks. One hour prior to addition of ^{64}Cu-ATSM, cells in the survival experiments were pretreated under anoxic conditions in a manner similar to previous studies [50]. Once anoxic preparation was complete, various levels of ^{64}Cu-ATSM activity were added and well mixed into cell culture medium. Cells were then incubated in hypoxic conditions for three hours to allow cellular uptake and for the hypoxic chamber to reach minimal oxygen concentration. After three hours all cells were transferred to normoxic conditions and incubated for seven days. Colonies were stained with crystal violet solution as previously described and those with approx. 50 cells or greater were scored as survivors. Each experiment using a determined activity was performed at least three times.

γH2AX Foci Formation Assay

10B2 and xrs-5 cell lines were synchronized on chamber slides in the G0/G1 phase by mitotic shake off. Following ^{64}Cu-ATSM incubation, cells were fixed for 15 minutes in 4 % paraformaldehyde, phosphate buffered saline (PBS) washed three times

(10 minutes each), permeabilized for 5 min in 0.2% Triton X-100 (Sigma, St Louis, MO) PBS solution, and blocked overnight at 48°C in 10% goat serum PBS solution. Cells were then incubated with anti-c-H2AX mouse monoclonal antibody (Millipore, Billerica, MA) for 1 hour, PBS washed three times (10 minutes each), and incubated for 1 hour at 37°C with secondary antibody Alexa Fluor-conjugated goat anti-mouse (Invitrogen, Grand Island, NY). Cells were then PBS washed four times (10 minutes each) and mounted with ProLong Gold Antifade Reagent with DAPI (Invitrogen). Fluorescence images were captured using a Zeiss Axioskop motorized z-stage fluorescent microscope (Olympus, Tokyo, Japan). One-micron thick z-stack images were obtained by Metamorph 7 (Molecular Devices, Sunnyvale, CA) software. Three independent experiments were performed. Manual counting was performed for foci analysis.

Chromosomal Aberration Assay

10B2 and xrs-5 cell lines were synchronized on well plate slides in the G0/G1 phase by mitotic shake off. Cells were then incubated under normoxic conditions for two hours before ^{64}Cu-ATSM and 0.1 µg/mL Colcemid (Invitrogen) was added to arrest cells in metaphase. After these additions, cells were incubated for three hours under hypoxic conditions and then for 12-16 hours under normoxic conditions. Cells were then treated with hypotonic solution (75 mM KCl) for 20 min at 37°C and fixed with methanol: acetic acid (3:1) solution for three cycles before being dropped onto slides. Samples were stained with 5% (v/v) Giemsa solution in Gurr (Wako). At least 50 metaphase cells were scored in three separate experiments. Chromosomal aberrations were quantified and classified as various chromosome and chromatid type aberrations.

^{64}Cu-ATSM Uptake

Incorporation of ^{64}Cu into cells was determined using liquid scintillation counting (LSC). LSC is a radiation detection/counting technique traditionally used for measuring low activity, beta-emitting radionuclides, and/or radioactivity in liquid form. Liquid samples containing ^{64}Cu were mixed with LSC cocktail containing solvent molecules and chemical scintillators. When a radionuclide decays in the LSC mixture, energy is absorbed by solvent molecules. This excites the solvent molecules, which then are able to transfer energy to the scintillators. These scintillators become excited, and once they transition back to a ground state a photon in the visible spectra is emitted in the solution. Photomultiplier tubes surround the sample and detect photons emitted. When standardized and calibrated properly, LSC instruments are able to count photons emitted from a sample, and these counts can be converted to the activity of the sample (Figure 17).

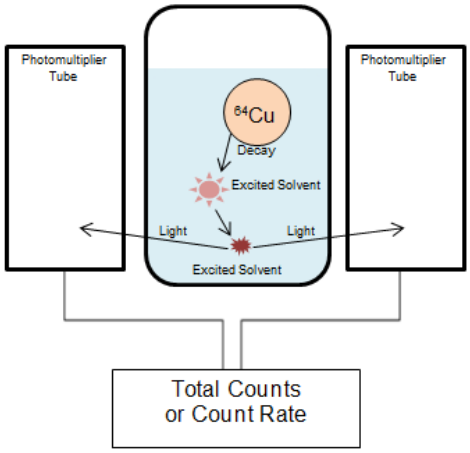

Figure 17: A liquid scintillation counter (LSC) works by energy absorbed in the LSC cocktail being detected as light.

10B2 and xrs-5 cells were plated at approx. 200,000 cells per 60 mm cell culture dish (Greiner Bio-One) in 4 mL of media three hours prior to experiments. Cells to be incubated with ^{64}Cu-ATSM in hypoxic and anoxic conditions were pretreated in anoxic conditions one hour prior to addition of activity. 185,000 Bq (5 µCi) of ^{64}Cu-ATSM was then added and mixed into cell cultures before three hours of incubation under the three –oxic conditions. After incubation, media was emptied into 20 mL glass LSC vials containing 5 mL Ultima Gold liquid scintillation cocktail (vial) (PerkinElmer, Waltham, MA). Cells were then washed with 4 mL PBS and emptied into a separate vial. Cells were then trypsinized with 1 mL Trypsin-EDTA (Hyclone, ThermoFisher, Waltham, MA) and added with 3 mL PBS to a vial. Activity present in trypsin was assumed to solely result from cellular incorporation of ^{64}Cu. Vials were shaken and counted on a Beckman LS-5801 liquid scintillation counter (Beckman Coulter, Brea, CA) using the full channel window. Quench differences between the vial compositions were accounted for to determine relative activity in the media, PBS, and trypsin containing vials.

RESULTS

Colony Formation Assay

Survival curves for 10B2 cells showed separation when irradiated with radiations of varied known LETs while those of xrs-5 cells dig not differ significantly with LET (Figure 18). D_{10} values for 10B2 ranged from 1.83 to 6.37 Gy while values for xrs-5 deviated very little from 1.00 to 1.18 Gy (iron and gamma irradiation, respectively) (Table 3). Ratios of D_{10} doses (10B2/xrs-5) were evaluated and used as a relative metric for the LET of the radiation with lower ratios, closer to the carbon SOBP or iron, indicating higher LET. Survival curves for cells exposed to ^{64}Cu-ATSM showed a D_{10} ratio just higher than that of the carbon SOBP (Figure 19).

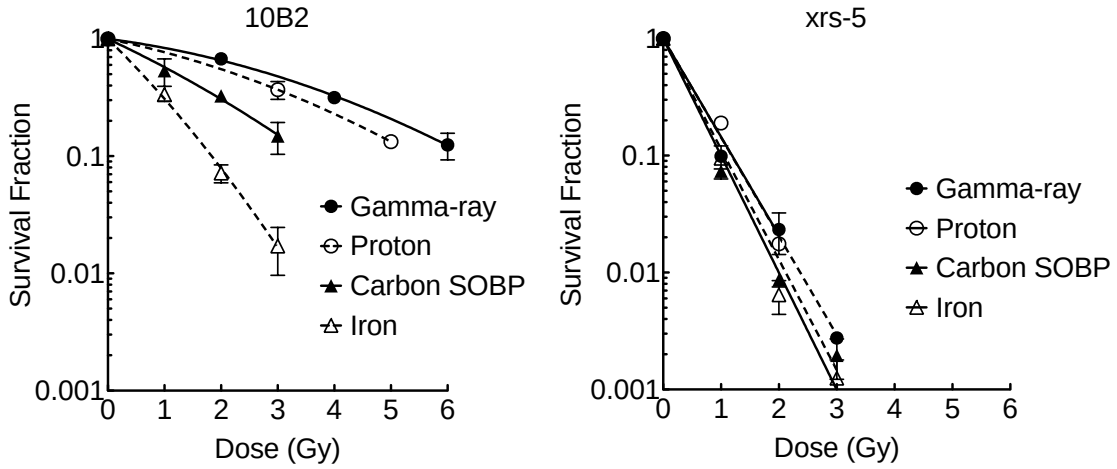

Figure 18: Survival curves of 10B2 and xrs-5 cells exposed to radiations of varying LETs. Gamma irradiation was performed under hypoxic conditions, while proton, carbon SOBP, and iron irradiation were performed in standard room conditions.

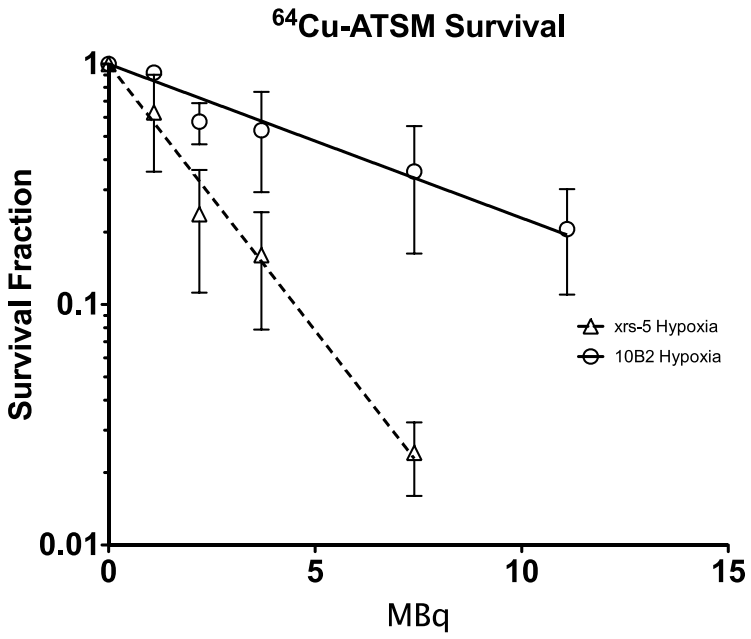

Figure 19: Linear survival curves of both 10B2 and xrs-5 cells exposed to ^{64}Cu-ATSM and incubated in hypoxia. Activity of ^{64}Cu added was used on the x-axis.

Table 3: D_{10} Doses and Ratios for Colony Formation Assay

Radiation	D_{10}: 10B2	D_{10}: xrs-5	10B2/xrs-5 D_{10} Ratio
Gamma	6.37 Gy	1.18 Gy	5.40
Proton	5.47 Gy	1.16 Gy	4.72
Carbon	3.55 Gy	1.05 Gy	3.38
Iron	1.83 Gy	1.00 Gy	1.83
^{64}Cu-ATSM	15.62 MBq	4.51 MBq	3.46

γH2AX Foci Formation Assay

Cells were incubated with ^{64}Cu-ATSM under hypoxic conditions, stained, imaged, and counted for γH2AX foci as a DNA DSB marker. Each point of cell type and activity on Figure 20 was the average of at least three foci analysis of 50 or more cells, and

error bars represent the standard error of the mean. Background foci levels, as determined by a linear fit [51], were 9.9 and 23.9 foci per cell for 10B2 and xrs-5 cells, respectively. The increase in foci per cell per MBq was calculated as 0.9 and 1.8 for 10B2 and xrs-5 cells, respectively.

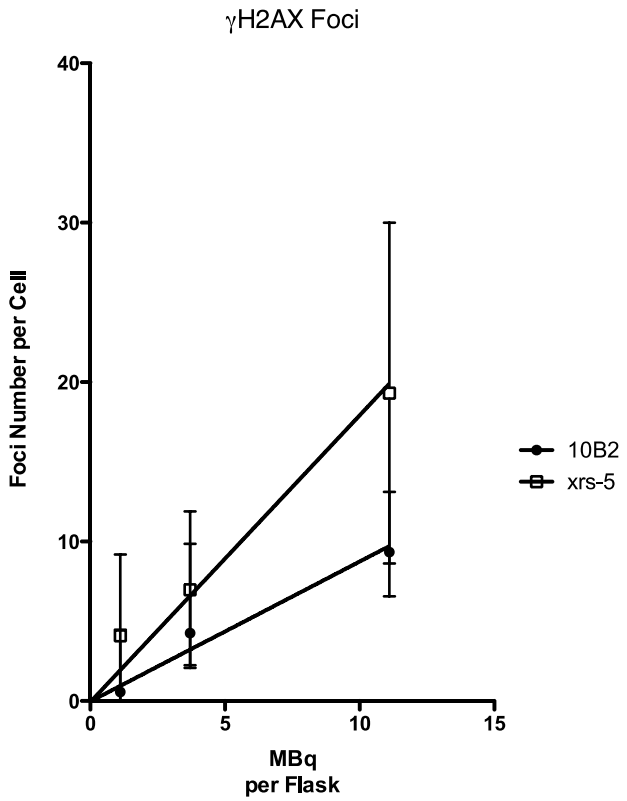

Figure 20: Foci response of cells incubated with varied activities normalized to background. Points are the mean of three plus experiments while the error bars represent standard error of the mean.

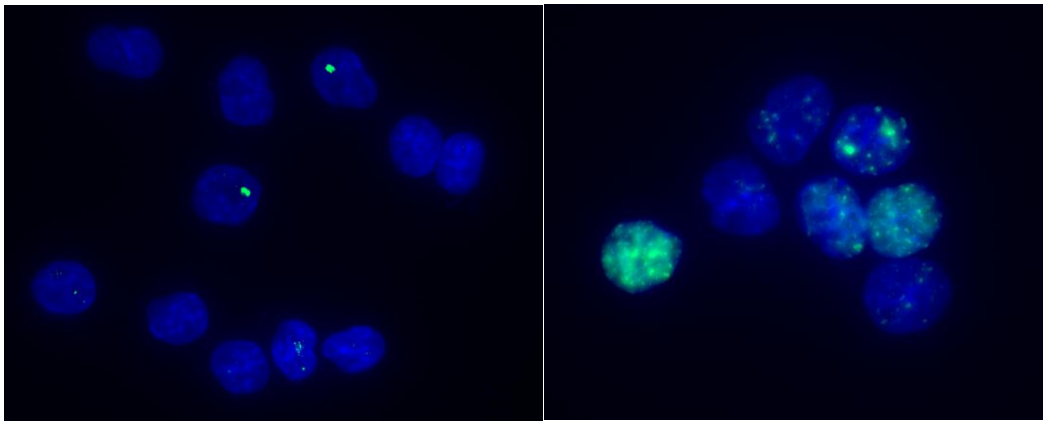

Figure 21: Foci images of 10B2 cells in control conditions (left) and high activity, 11.1 MBq (right).

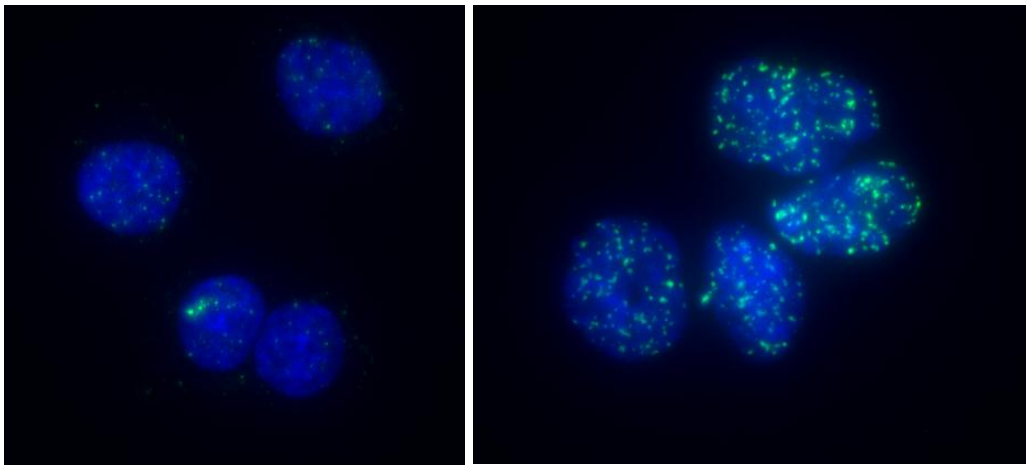

Figure 22: Foci images for xrs-5 cells in control conditions (left) and high activity, 11.1 MBq (right).

Chromosomal Aberration Assay

Chromosomes of 10B2 and xrs-5 cells were stained and counted for both chromosome (from G0/G1 phase damage) and chromatid (from S/G2 phase damage) type aberrations (Figures 23 & 24). At least 50 metaphases spreads were counted for each condition listed. Cells exhibited both types of aberrations, indicating DNA damage which occurred both before and after DNA was replicated, although cells were initially

synchronous in the G1 phase [8]. 10B2 cells exhibited general increases in chromatid type aberrations (gaps, breaks, isochromatid deletion, and exchanges) with increasing activity, while chromosome aberrations (acentric rings, terminal deletions, centric rings, and dicentrics) showed an activity response for dicentric and acentric rings (Table 4).

Chromatid aberrations for xrs-5 cells were significantly greater for than 10B2 cells at similar activities while the presence of chromosome type aberrations were similar (Table 5). Significantly, the damage to chromosomes observed in the two highest activity experiments yielded metaphase spreads with damage extensive enough to prohibit chromosome aberration qualification and quantification.

Both cell types showed complex chromosomal aberrations. Though not directly quantified, these are typically combinations of three of more chromosomes and consist of multiple chromosomal aberrations [52]. They are typically associated with high LET radiation [53].

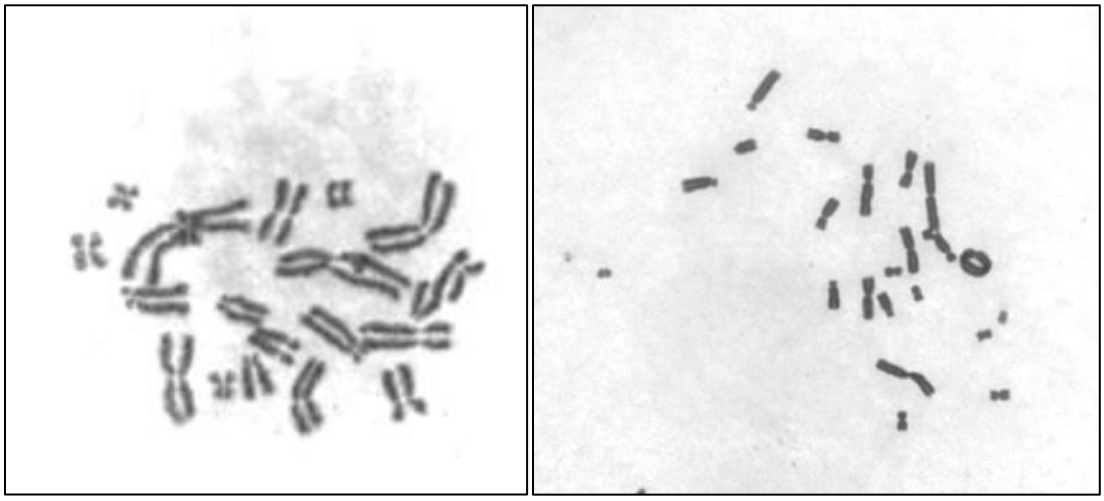

Figure 23: Control 10B2 metaphase spread (left), metaphase spread of cells exposed to 11.1 MBq (right). The spread on the right displays a clear centric ring and dicentric.

Table 4: 10B2 Chromosomal Aberrations

10B2	Chromatid Aberrations				Chromosome Aberrations			
Dose	Gap	Break	Iso	Exc	Acentric ring	Tem del	Cent ring	Dicentric
control	0.033	0.0067	0.0033	0	0.013	0.0067	0	0
1.1 MBq (30 µCi)	0.05	0.03	0.023	0	0.033	0.0033	0.0067	0.01
3.7 MBq (100 µCi)	0.11	0.17	0.11	0.13	0.067	0.017	0.017	0.0067
11.1 MBq (300 µCi)	0.14	0.32	0.16	0.17	0.063	0.003	0.0097	0.033

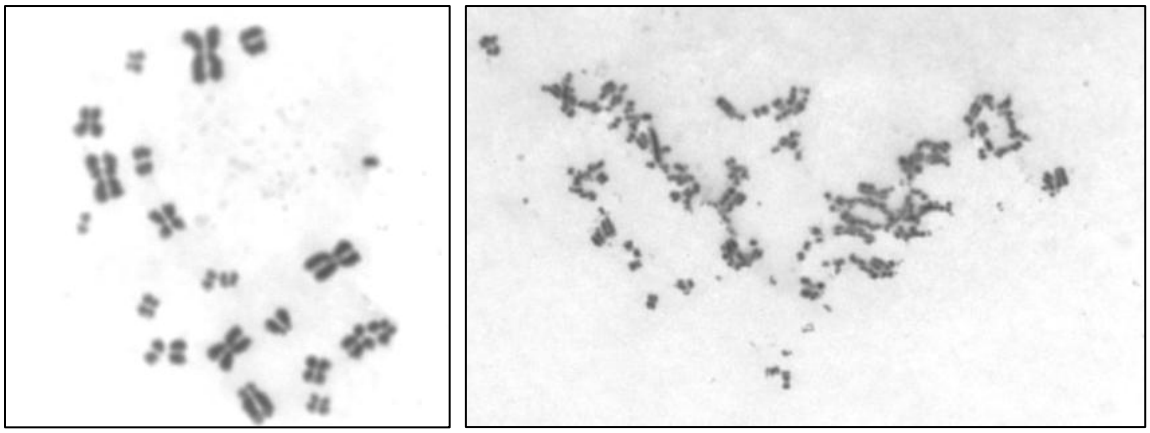

Figure 24: Control xrs-5 metaphase spread (left) and representative spread of chromosomes for xrs-5 cells in 11.1 MBq experiement (right). Damage was extensive enough to prohibit evaluation of definative chromosomal aberrations for two high activity experiments.

Table 5: xrs-5 Chromosomal Aberrations

xrs-5	Chromatid Aberrations				Chromosome Aberrations			
Dose	Gap	Break	Iso	Exc	Acentric ring	Tem del	Cent ring	Dicentric
control	0.23	0.12	0.13	0.021	0.017	0	0.0055	0.016
1.1 MBq (30 µCi)	0.58	0.96	0.19	0.27	0.01	0	0.016	0.005
3.7 MBq (100 µCi)	N/A	N/A	N/A	N/A	N/A	N/A	N/A	N/A
11.1 MBq (300 µCi)	N/A	N/A	N/A	N/A	N/A	N/A	N/A	N/A

Table 5: Chromosome aberrations of various types for xrs-5 cells incubated with ^{64}Cu-ATSM.

^{64}Cu-ATSM Uptake

Twenty seven cell lines were evaluated for uptake of ^{64}Cu activity in all three -oxic conditions (Figure 25). Cells of CHO and human origin have been typed as to their origin (Table 6), while the majority of canine origins have been identified (Table 7). Human and CHO cells showed similar ^{64}Cu uptake under all three –oxic conditions. Canine normal cells generally showed slightly higher uptake in the anoxic conditions, while canine cancer cells showed significantly higher uptake in the hypoxic state than the other two states. The metric of Bq/cell was utilized to account for differences in cell number between cell lines when they were plated. Because this assay was used to gain general understanding of uptake characteristics of cell lines and not determine statistically significant differences, statistical hypothesis tests were not performed.

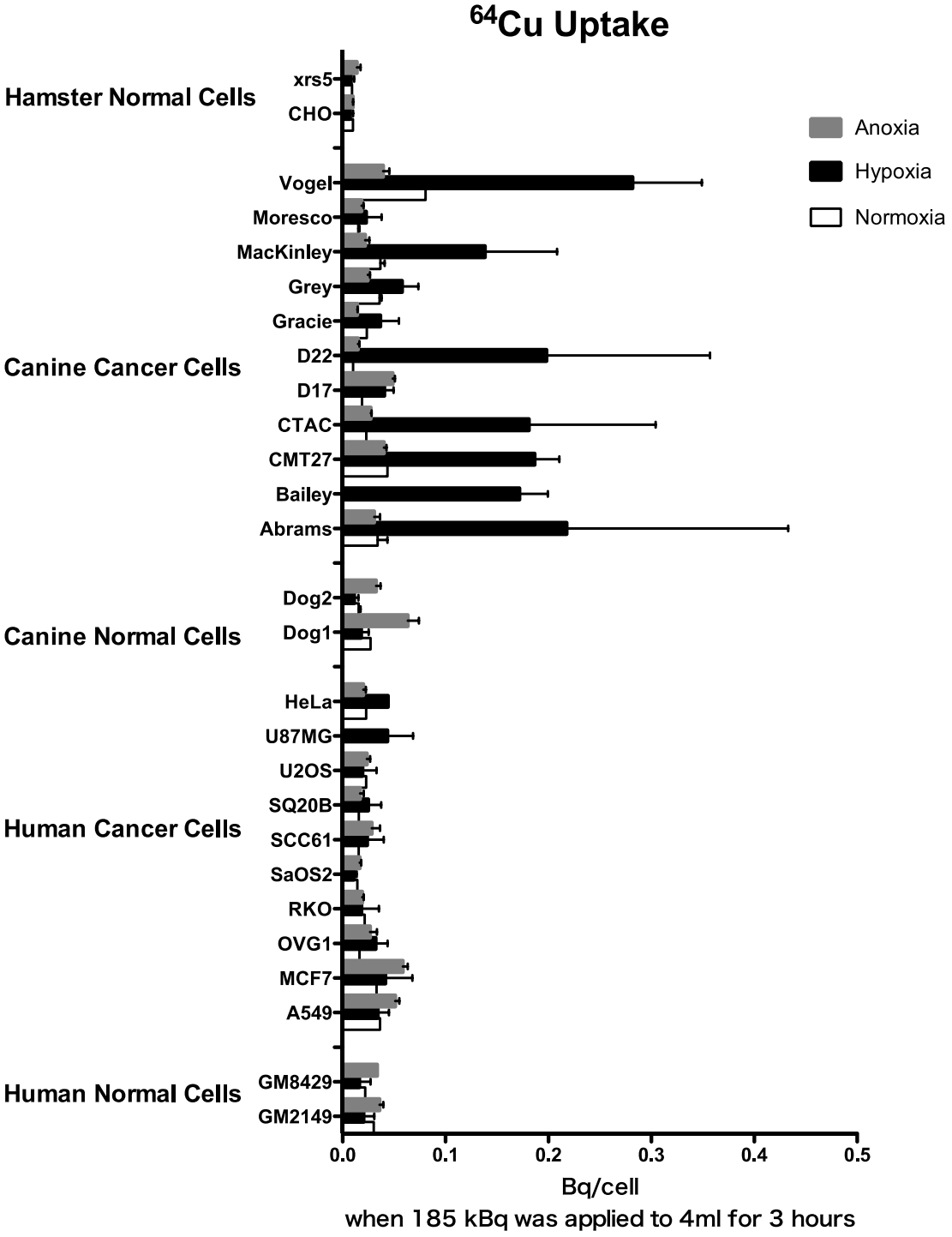

Figure 25: Uptake of ^{64}Cu into various cells when incubated for three hours under anoxic, hypoxic, and normoxic conditions. Error bars represent standard error of the mean.

Table 6: CHO & Human Cell Lines for Uptake

CHO	Type	Human Normal	Type	Human Cancer	Type
10B2	Wild-type	GM8429	Fibroblast	A549	Lung Adenocarcinoma
xrs-5	NHEJ mutant	GM2149	Fibroblast	MCF7	Breast Adenocarcinoma
				OVG1	Ovarian Carcinoma
				RKO	Colon Carcinoma
				SaOS-2	Osteosarcoma
				SCC61	Head & Neck Squamous Cell Carcinoma
				SQ20B	Head & Neck Squamous Cell Carcinoma
				U2OS	Osteosarcoma
				U87MG	Glioblastoma

Table 7: Canine Cell Lines for Uptake

Canine Normal	Type	Canine Cancer	Type
Dog 1	Fibroblast	Abrams	Osteosarcoma
Dog 2	Fibroblast	Bailey	N/A
		CMT27	Mammary Adenocarcinoma
		CTAC	Thyroid Adenocarcinoma
		D17	Osteosarcoma
		D22	Osteosarcoma
		Gracie	Osteosarcoma
		Grey	Osteosarcoma
		MacKinley	Osteosarcoma
		Moresco	Osteosarcoma
		Vogel	Osteosarcoma

DISCUSSION

Colony Formation Assay

Colony formation results indicate cell kill from ^{64}Cu is due to high LET radiation as the D_{10} ratio of ^{64}Cu-ATSM and carbon SOBP experiments were similar. Though the absolute values of the D_{10}'s do not provide a definitive value of the LET of the radiation, these results do provide a relative scale upon which to consider the LET of a radiation when the two CHO cell lines were exposed to the same dose or activity. More refined quantification of ^{64}Cu-ATSM's relative LET would be difficult to attain in a biological setting because LET is definitively a physical parameter. Only by modeling how cells are killed relative to this physical parameter was an estimate of LET attained here. By using this strategy to model how the two CHO cell lines behave in response to varied LET radiations, the LET of ^{64}Cu conjugated with ATSM is roughly estimated to lie between that of the proton and carbon SOBP radiations used, approx. 1 and 70 respectively. Given the LET of Auger electrons is estimated to be between 3 and 25 keV/μm [54], the D_{10} ratios support the prominent role of high LET Auger electrons in cell killing, as all other emissions of ^{64}Cu display low LET. In addition to the D_{10} ratio indicating high LET radiation causing cell death, cell survival curve fitting of ^{64}Cu-ATSM experiments also signified high LET radiation damage. Fitting the 10B2 ^{64}Cu-ATSM survival curve using a linear fit was more representative of the data than a linear-quadratic fit. Hypoxic conditions (as used for ^{64}Cu-ATSM) would typically skew a survival curve to be more linear-quadratic, high LET radiation make survival curves more linear compared with a low LET radiation [8], and DNA repair proficient cell lines typically have linear-quadratic survival curves. These characteristics of the linear 10B2

^{64}Cu-ATSM survival curve fit make it appear more likely high LET radiation was damaging the ^{64}Cu-ATSM incubated cells.

Because the D_{10} of ^{64}Cu-ATSM is compared to standard radiations, it is worthwhile to mention procedural differences in colony formation experiments between standard radiations and ^{64}Cu-ATSM experiments. While ^{64}Cu-ATSM experiments were performed in hypoxia, those of the standard radiations were performed in standard room temperature conditions. This difference was mandated due to limitations prohibiting irradiation of cells at the NIRS facilities with proton, carbon SOBP, and iron under hypoxic conditions, while ^{137}Cs irradiation was performed in standard room conditions to maintain consistency with the other standard irradiations. Specifically, cell flask targets and dosimetry was not available for irradiating cells in hypoxic chambers (or other methods to achieve hypoxia) at the NIRS. This difference in –oxic conditions during irradiation may have had a more significant effect on the lower LET irradiations (^{137}Cs and protons) but less effect on the higher LET radiations (carbon SOBP, iron). This effect would be manifested due to a high oxygen enhancement ratio (OER) in colony formation assays for low LET radiations [8, 55]. Because the D_{10} ratio of ^{64}Cu-ATSM experiments were close to those of carbon SOBP, indicating high LET and a low OER, this experimental difference was not considered significant for interpreting results.

Another variance between the colony formation assays for the standard radiations and that of ^{64}Cu-ATSM was the duration of irradiation. While the period of irradiation for the standard radiations were of short duration, irradiation of ^{64}Cu exposed cells occurred during the full week of colony formation experiments. Long term irradiation of cells by ^{64}Cu likely resulted in different DNA DSB repair dynamics than the

short term standard irradiations [8]. Although this difference might suggest more DNA repair would be possible in the case of ^{64}Cu incubated cells, especially because of the potential for dose delivery at a lower rate [56], the dosimetry of the ^{64}Cu irradiation conditions are not well enough known to be conclusive. Since the ^{64}Cu nuclide can deliver large radiation doses close to the nucleus if it decays close to the nucleus with Auger emissions [50, 57] it would be difficult to ascertain the dose rate of ^{64}Cu-ATSM during these experiments.

γH2AX Foci Formation Assay

Quantitative results of the γH2AX experiments showed a linear increase in foci formation for both CHO cell lines, with a more rapid increase in the NHEJ mutant xrs-5 cell line. This was an expected result, as the mutant cell line is not as effectively able to repair DSBs produced by increasing ^{64}Cu activity as the normal line. Background levels of γH2AX were observed higher than previously reported [58, 59]. While this may be due to personnel counting discrepancies, more likely explanations are incubation in hypoxia and close to ^{64}Cu-ATSM γH2AX experiments likely increased DNA DSBs of controls. Incubation of cells in hypoxia creates biological stress producing DSBs [60], and incubation of controls in a high radiation background would also raise background levels of γH2AX for both cell lines.

A high degree of variability, as indicated by standard errors of the mean for both cell lines, was observed in γH2AX foci analysis. Highly and lightly damaged cells, such as those seen in Figure 21, 11.1 MBq represent such variation. Highly damaged cells were presumed to result from cells being fixed and stained in S phase or cells having

heterogeneously higher ^{64}Cu uptake. In S phase, DNA damage and DSBs intrinsically occur due to mechanisms of DNA replication, and staining cells in this phase shows damage from the DNA replication process. Cells thought to be stained in S phase had less distinct foci than other cells, but were still counter in order to take into account all variability in foci or DNA damage expression. Other cells with higher uptake often had more definitive foci than the S phase cells, but still showed extensive damage. Opposed to these highly damaged cells were cells that showed little damage relative to other cells in the same experimental conditions. Low ^{64}Cu uptake or poor cellular staining was thought to explain γH2AX staining in these cells. That γH2AX images of single cells displaying great heterogeneity in quantity of foci under the same experimental conditions indicates other factors than oxygen status play a role in the extent Cu-ATSM is able to incorporate into damage cells.

In addition to the quantitative results, a qualitative observation was made that many ^{64}Cu-ATSM incubated cells, both 10B2 and xrs-5, had what appeared to be large and intense foci regions. These were thought to be multiple clustered γH2AX foci, potentially resulting from an Auger cascade. To evaluate this further, a formal comparison between traditional gamma irradiation and ^{64}Cu-ATSM treatment to further elucidate how sizes of foci differ may provide more definitive data showing that these large foci are indeed clusters of individual foci.

Chromosomal Aberration Assay

The results of the chromosome aberration studies showed complex DNA damage when CHO cell lines were incubated with ^{64}Cu-ATSM. This was most readily

apparent in the xrs-5 experiments. The low activity xrs-5 experiments yielded quantifiable chromosomal damage, while high activity experiments resulted in damage extending to the point of unrecognizable aberrations. No activity response for chromosome type aberrations in xrs-5 were observed as only one experiment (1.1 MBq) with ^{64}Cu-ATSM was quantifiable. The chromatid type aberrations seen in both xrs-5 and 10B2 cells indicate that though cells were synchronized in G0/G1 phase some went past the G2 phase. This may have occurred by damaged cells bypassing a G1 DNA damage checkpoint [61] or more likely occurred when cells were able to cycle past the G1 phase relatively undamaged only to be damaged in S or G2 phases. Increased occurrence of chromatid type aberrations with activity for both cell lines and increased chromosome type aberrations in 10B2 cells are consistent with normal dose response (i.e. more damage at higher doses). Chromosome type aberrations are acutely lethal [8], which would not allow them to increase as readily as chromatid type damage with increasing dose.

Both 10B2 and xrs-5 cells also showed complex chromosome aberrations. These are typically observed with high LET radiation [45, 46, 53]. Because colony formation assays were the main focus of this research and chromosomal aberrations provided supplementary DNA damage information complete analysis of complex chromosomal rearrangements were not performed. The presence of complex DNA damage does serve to indicate high LET Auger electrons do play a role in chromosomal damage, but more extensive analysis would be needed to quantify these complex chromosomal rearrangements.

^{64}Cu-ATSM Uptake

For uptake experiments the convention of Bq per cell was utilized to control for variation in number of cells plated between cell lines. In these experiments it was surprising to see similar uptake in all –oxic conditions for human cells, as previous reports have shown noticeably higher uptake in hypoxic or anoxic conditions *in vitro* [33, 62]. One reason for the similar uptake between –oxic conditions for most cell lines is the lack of a driving –oxic gradient *in vitro*. *In vivo* Cu-ATSM has a preference to unload in hypoxic tissue relative to normoxic tissue or oxygenated blood. In our experimental setup that –gradient did not exist, as the oxygen level in cell culture media changed –oxic levels at the same rate cells did, allowing no oxygen gradient making it preferential for Cu-ATSM to dissociate inside cells. This theory does not explain why previous studies *in vitro* showed higher uptake in hypoxic conditions, but results of higher uptake in cancerous canine cell lines under hypoxic conditions shows some cell lines do uptake better in hypoxia. The noticeably higher uptake in hypoxic canine cancer cell experiments was also unanticipated. Many of the cancerous canine cell line were osteosarcomas, but the human osteosarcoma cell lines displayed low ^{64}Cu uptake. Although ^{64}Cu-ATSM imaging experiments have been performed using canine models [63, 64] the observation of increased uptake in hypoxic canine cancer cells, experiments typically performed *in vitro*, has not been observed.

Because physical oxygen concentration does not explain the higher uptake in canine cancer cell lines under hypoxia, an explanation likely lies in unique biological characteristics of these cell lines. Cu-ATSM is known to be reduced by the electron transport chain of mitochondria [29, 65], so potential distinctive traits of cancerous

canine electron transport chains may result in this difference. Though Cu-ATSM is generally thought to cross cellular membranes easily due to its lipophilicity there may be Cu transporter mechanisms in these cell lines with increased Cu uptake in hypoxia allowing them to incorporate more Cu [62].

Future Directions

While the colony formation assay results provide strong support for Auger electrons causing cell death, and chromosomal aberration and γH2AX results provide auxiliary evidence, additional studies would prove beneficial in further understanding how dose is deposited in hypoxic cells. One such method to assay presence of ^{64}Cu activity in cells after incubation under various –oxic conditions would be autoradiography [66]. Using this technique positron, beta, and gamma emissions from ^{64}Cu inside cells would be readily detectable and provide evidence of subcellular radionuclide localization [67]. While evidence is presently available on subcellular ^{64}Cu localization using Cu-ATSM [50, 68], performing autoradiography with numerous cell lines would be useful for comparing uptake results from this experiment to an alternative assay. This type of experiment would also be useful for evaluating uptake heterogeneity between cells. Autoradiography could be applied to either *in vitro* or *in vivo* experiments using a tumor cross section [69].

Much of this research was performed considering the activity of ^{64}Cu-ATSM used in experiments, but estimating dose to cells would be a valuable and complementary avenue of research. On a cellular level, dose estimation would be difficult analytically because of the various radiations emitted by ^{64}Cu, but Monte Carlo methods would be

an fitting approach for dose estimation [70]. Using subcellular ^{64}Cu concentration and cellular uptake data [50, 68], decay of subcellular ^{64}Cu could be simulated and energy deposition in various regions of the cell, most importantly the nucleus, could be estimated.

In addition to Cu-ATSM preferentially localizing to hypoxic tumor regions, the agent may also serve the purpose of localizing to cancer stem cells, as these are hypothesized to be located in hypoxic regions [71, 72]. Cancer stem cells in hypoxic regions are thought to occur due to HIF expression in hypoxic regions. HIFs are transcription factors which promote altered gene expression in hypoxia, and some of these gene alterations are associated with cell renewal and variable differentiation capabilities [72]. Due to this association between hypoxia and cancer stem cells, research evaluating how Cu-ATSM may uptake or damage these cells, as defined by specific cell surface markers [73, 74], would be intriguing.

CONCLUSIONS

Tumors containing hypoxic tissue regions are resistant to many cancer therapy modalities. It was thought Auger electrons would be predominant in cell killing and DNA damage, and experiments were designed to test this theory and provide other results worthwhile for considering radiotherapy applications with ^{64}Cu-ATSM. By evaluating the ^{64}Cu-ATSM agent in cell culture, various characteristics have been observed that provide evidence for DNA and cell damaging effects which may prove useful for nuclide radiotherapy. Cell survival using a CHO model system showed the effective radiation in the ^{64}Cu-ATSM agent kills cells in a high LET manner, which would be useful for damaging hypoxic tumor cells. Both chromosome aberration assays and γH2AX foci formation assays showed the ^{64}Cu-ATSM agent capable of damaging chromosomes in a complex manner and creating DSBs, potentially in a clustered way indicative of highly localized energy deposition from Auger electron cascades. Uptake results indicate CHO and human cell lines incorporate ^{64}Cu-ATSM similarly in various –oxic states. Cancerous canine cell lines, many of which were osteosarcomas, displayed higher uptake than other cell lines and had generally higher uptake in hypoxia. These experimental results indicate use of ^{64}Cu-ATSM in radiotherapy of tumor hypoxia to be viable from a biological perspective. Further study both *in vitro* and *in vivo* to more readily define optimal and effective use of ^{64}Cu-ATSM for radiotherapy is warranted.

REFERENCES

1. Pacelli, R., et al., *Radiation therapy following surgery for localized breast cancer: outcome prediction by classical prognostic factors and approximated genetic subtypes.* Journal of radiation research, 2013. **54**(2): p. 292-298.
2. Brizel, D.M., et al., *Tumor hypoxia adversely affects the prognosis of carcinoma of the head and neck.* International Journal of Radiation Oncology* Biology* Physics, 1997. **38**(2): p. 285-289.
3. Isa, A.Y., et al., *Hypoxia in head and neck cancer.* 2014.
4. Bayer, C. and P. Vaupel, *Acute versus chronic hypoxia in tumors.* Strahlentherapie und Onkologie, 2012. **188**(7): p. 616-627.
5. Bayer, C., et al., *Acute versus chronic hypoxia: why a simplified classification is simply not enough.* International Journal of Radiation Oncology* Biology* Physics, 2011. **80**(4): p. 965-968.
6. Brown, J.M., *The Hypoxic Cell A Target for Selective Cancer Therapy—Eighteenth Bruce F. Cain Memorial Award Lecture.* Cancer Research, 1999. **59**(23): p. 5863-5870.
7. Cuenod, C., et al., *Tumor angiogenesis: pathophysiology and implications for contrast-enhanced MRI and CT assessment.* Abdominal imaging, 2006. **31**(2): p. 188-193.
8. Hall, E.J. and A.J. Giaccia, *Radiobiology for the Radiologist*. 2006: Lippincott Williams & Wilkins.

9. Le, Q.-T., et al., *Comparison of the comet assay and the oxygen microelectrode for measuring tumor oxygenation in head-and-neck cancer patients.* International Journal of Radiation Oncology* Biology* Physics, 2003. **56**(2): p. 375-383.

10. Lee, J.-W., et al., *Hypoxia-inducible factor (HIF-1) α: its protein stability and biological functions.* Experimental & molecular medicine, 2004. **36**(1): p. 1-12.

11. Semenza, G.L., *HIF-1 mediates the Warburg effect in clear cell renal carcinoma.* Journal of bioenergetics and biomembranes, 2007. **39**(3): p. 231-234.

12. Song, C.W., H. Park, and R.J. Griffin, *Improvement of tumor oxygenation by mild hyperthermia.* Radiation research, 2001. **155**(4): p. 515-528.

13. Dische, S., et al., *Carcinoma of the cervix—anaemia, radiotherapy and hyperbaric oxygen.* The British journal of radiology, 1983. **56**(664): p. 251-255.

14. Matsumoto, S., et al., *Antiangiogenic agent sunitinib transiently increases tumor oxygenation and suppresses cycling hypoxia.* Cancer research, 2011. **71**(20): p. 6350-6359.

15. Karroum, O., et al., *Tumor reoxygenation following administration of Mitogen-Activated Protein Kinase inhibitors: A rationale for combination with radiation therapy.* Radiotherapy and Oncology, 2012. **105**(1): p. 64-71.

16. Karroum, O., et al., *Tumor Reoxygenation Following Administration of the EGFR Inhibitor, Gefitinib, in Experimental Tumors*, in *Oxygen Transport to Tissue XXXV*. 2013, Springer. p. 265-271.

17. Semenza, G.L., *Targeting HIF-1 for cancer therapy.* Nature Reviews Cancer, 2003. **3**(10): p. 721-732.

18. Turner, J.E., *Atoms, radiation, and radiation protection*. 2008: John Wiley & Sons.

19. Michaels, H.B. and J.W. Hunt, *A model for radiation damage in cells by direct effect and by indirect effect: a radiation chemistry approach.* Radiation research, 1978. **74**(1): p. 23-34.

20. Knoll, G.F., *Radiation detection and measurement*. 2010: John Wiley & Sons.

21. Goodhead, D.T., *Mechanisms for the biological effectiveness of high-LET radiations.* Journal of radiation research, 1999. **40**(Suppl): p. S1-S13.

22. Kanai, T., et al., *Irradiation of mixed beam and design of spread-out Bragg peak for heavy-ion radiotherapy.* Radiation research, 1997. **147**(1): p. 78-85.

23. Volkert, W., et al., *Therapeutic radionuclides: production and decay property considerations.* Journal of nuclear medicine: official publication, Society of Nuclear Medicine, 1991. **32**(1): p. 174-185.

24. Spinks, J.W.T. and R.J. Woods, *Introduction to radiation chemistry.* 1976.

25. Chan, P., et al., *The Radiotoxicity of Iodine-125 in Mammalian Cells: II. A Comparative Study on Cell Survival and Cytogenetic Responses to125 IUdR, ^131\rmIUdR, and ^3\rmHTdR.* Radiation research, 1976. **67**(2): p. 332-343.

26. Adelstein, S., *Merrill C. Sosman Lecture. The Auger process: a therapeutic promise?* AJR. American journal of roentgenology, 1993. **160**(4): p. 707-713.

27. Ter-Pogossian, M.M., *Positron emission tomography (PET)*, in *Diagnostic Imaging in Medicine*. 1983, Springer. p. 273-277.

28. Miller, P.W., et al., *Synthesis of 11C, 18F, 15O, and 13N radiolabels for positron emission tomography.* Angewandte Chemie International Edition, 2008. **47**(47): p. 8998-9033.

29. Fujibayashi, Y., et al., *Copper-62-ATSM: a new hypoxia imaging agent with high membrane permeability and low redox potential.* Journal of nuclear medicine: official publication, Society of Nuclear Medicine, 1997. **38**(7): p. 1155-1160.

30. Dearling, J.L., et al., *Copper bis (thiosemicarbazone) complexes as hypoxia imaging agents: structure-activity relationships.* JBIC Journal of Biological Inorganic Chemistry, 2002. **7**(3): p. 249-259.

31. Maurer, R.I., et al., *Studies on the mechanism of hypoxic selectivity in copper bis (thiosemicarbazone) radiopharmaceuticals.* Journal of medicinal chemistry, 2002. **45**(7): p. 1420-1431.

32. Vāvere, A.L. and J.S. Lewis, *Cu–ATSM: A radiopharmaceutical for the PET imaging of hypoxia.* Dalton Transactions, 2007(43): p. 4893-4902.

33. Lewis, J.S., et al., *Evaluation of 64Cu-ATSM in vitro and in vivo in a hypoxic tumor model.* Journal of nuclear medicine: official publication, Society of Nuclear Medicine, 1999. **40**(1): p. 177-183.

34. Yuan, H., et al., *Intertumoral differences in hypoxia selectivity of the PET imaging agent 64Cu (II)-diacetyl-bis (N4-methylthiosemicarbazone).* Journal of Nuclear Medicine, 2006. **47**(6): p. 989-998.

35. Szelecsényi, F., et al., *Formation of< sup> 60</sup> Cu and< sup> 61</sup> Cu via Co+< sup> 3</sup> He reactions up to 70 MeV: production possibility of< sup> 60</sup> Cu for PET studies.* Nuclear Instruments and Methods in Physics

Research Section B: Beam Interactions with Materials and Atoms, 2004. **222**(3): p. 364-370.

36. Avila-Rodriguez, M.A., J.A. Nye, and R.J. Nickles, *Simultaneous production of high specific activity< sup> 64</sup> Cu and< sup> 61</sup> Co with 11.4 MeV protons on enriched< sup> 64</sup> Ni nuclei.* Applied Radiation and Isotopes, 2007. **65**(10): p. 1115-1120.

37. Robinson Jr, G., F. Zielinski, and A. Lee, *The zinc-62/copper-62 generator: a convenient source of copper-62 for radiopharmaceuticals.* The International journal of applied radiation and isotopes, 1980. **31**(2): p. 111-116.

38. Dehdashti, F., et al., *Assessing tumor hypoxia in cervical cancer by positron emission tomography with< sup> 60</sup> Cu-ATSM: Relationship to therapeutic response—a preliminary report.* International Journal of Radiation Oncology* Biology* Physics, 2003. **55**(5): p. 1233-1238.

39. Lewis, J.S., et al., *Copper-64-diacetyl-bis (N4-methylthiosemicarbazone): An agent for radiotherapy.* Proceedings of the National Academy of Sciences, 2001. **98**(3): p. 1206-1211.

40. Rassool, F.V., *DNA double strand breaks (DSB) and non-homologous end joining (NHEJ) pathways in human leukemia.* Cancer letters, 2003. **193**(1): p. 1-9.

41. Peterson, S.R., et al., *Loss of the catalytic subunit of the DNA-dependent protein kinase in DNA double-strand-break-repair mutant mammalian cells.* Proceedings of the National Academy of Sciences, 1995. **92**(8): p. 3171-3174.

42. Thompson, L.H., *Recognition, signaling, and repair of DNA double-strand breaks produced by ionizing radiation in mammalian cells: the molecular choreography.* Mutation Research/Reviews in Mutation Research, 2012. **751**(2): p. 158-246.

43. Kuo, L.J. and L.-X. Yang, *γ-H2AX-a novel biomarker for DNA double-strand breaks.* In Vivo, 2008. **22**(3): p. 305-309.

44. Genet, S.C., et al., *Comparison of cellular lethality in DNA repair-proficient or-deficient cell lines resulting from exposure to 70 MeV/n protons or 290 MeV/n carbon ions.* Oncology reports, 2012. **28**(5): p. 1591-1596.

45. Hada, M. and A.G. Georgakilas, *Formation of clustered DNA damage after high-LET irradiation: a review.* Journal of radiation research, 2008. **49**(3): p. 203-210.

46. Leatherbarrow, E.L., et al., *Induction and quantification of γ-H2AX foci following low and high LET-irradiation.* International journal of radiation biology, 2006. **82**(2): p. 111-118.

47. Jeggo, P. and L. Kemp, *X-ray-sensitive mutants of Chinese hamster ovary cell line isolation and cross-sensitivity to other DNA-damaging agents.* Mutation Research/DNA Repair Reports, 1983. **112**(6): p. 313-327.

48. Hinz, J.M., et al., *Repression of mutagenesis by Rad51D-mediated homologous recombination.* Nucleic acids research, 2006. **34**(5): p. 1358-1368.

49. Gingras, B., R. Somorjai, and C. Bayley, *The preparation of some thiosemicarbazones and their copper complexes.* Canadian Journal of Chemistry, 1961. **39**(5): p. 973-985.

50. Obata, A., et al., *Basic characterization of< sup> 64</sup> Cu-ATSM as a radiotherapy agent.* Nuclear medicine and biology, 2005. **32**(1): p. 21-28.

51. Paull, T.T., et al., *A critical role for histone H2AX in recruitment of repair factors to nuclear foci after DNA damage.* Current Biology, 2000. **10**(15): p. 886-895.

52. Patsalis, P., *Complex chromosomal rearrangements.* Genetic counseling (Geneva, Switzerland), 2006. **18**(1): p. 57-69.

53. Durante, M., et al., *Complex chromosomal rearrangements induced in vivo by heavy ions.* Cytogenetic and genome research, 2004. **104**(1-4): p. 240-244.

54. Kassis, A.I., *The amazing world of Auger electrons.* International journal of radiation biology, 2004. **80**(11-12): p. 789-803.

55. Wenzl, T. and J.J. Wilkens, *Modelling of the oxygen enhancement ratio for ion beam radiation therapy.* Physics in medicine and biology, 2011. **56**(11): p. 3251.

56. Bedford, J.S. and J.B. Mitchell, *Dose-rate effects in synchronous mammalian cells in culture.* Radiation research, 1973. **54**(2): p. 316-327.

57. Wang, M., et al., *Subcellular Localization of Radiolabeled Somatostatin Analogues Implications for Targeted Radiotherapy of Cancer.* Cancer research, 2003. **63**(20): p. 6864-6869.

58. Kato, T.A., R. Okayasu, and J.S. Bedford, *Signatures of DNA double strand breaks produced in irradiated G1 and G2 cells persist into mitosis.* Journal of cellular physiology, 2009. **219**(3): p. 760-765.

59. Kato, T., et al., *Cytotoxicity of cigarette smoke condensate is not due to DNA double strand breaks: Comparative studies using radiosensitive mutant and wild-type CHO cells.* International journal of radiation biology, 2007. **83**(9): p. 583-591.

60. Bencokova, Z., et al., *ATM activation and signaling under hypoxic conditions.* Molecular and cellular biology, 2009. **29**(2): p. 526-537.

61. Iliakis, G., et al., *DNA damage checkpoint control in cells exposed to ionizing radiation.* Oncogene, 2003. **22**(37): p. 5834-5847.

62. Burgman, P., et al., *Cell line-dependent differences in uptake and retention of the hypoxia-selective nuclear imaging agent Cu-ATSM.* Nuclear medicine and biology, 2005. **32**(6): p. 623-630.

63. Hansen, A.E., et al., *(64) Cu-ATSM and (18) FDG PET uptake and (64) Cu-ATSM autoradiography in spontaneous canine tumors: comparison with pimonidazole hypoxia immunohistochemistry.* Radiation oncology, 2012. **7**(1): p. 89.

64. Lewis, J.S., et al., *Delineation of hypoxia in canine myocardium using PET and copper (II)-diacetyl-bis (N4-methylthiosemicarbazone).* Journal of Nuclear Medicine, 2002. **43**(11): p. 1557-1569.

65. Obata, A., et al., *Retention mechanism of hypoxia selective nuclear imaging/radiotherapeutic agent Cu-diacetyl-bis (N 4-methylthiosemicarbazone)(Cu-ATSM) in tumor cells.* Annals of nuclear medicine, 2001. **15**(6): p. 499-504.

66. Gahan, P., *Autoradiography for biologists*. 2012: Elsevier.

67. Stumpf, W.E., *Cellular and subcellular 3H-estradiol localization in the pituitary by autoradiography.* Zeitschrift für Zellforschung und Mikroskopische Anatomie, 1968. **92**(1): p. 23-33.

68. Baerga, I.D., R.P. Maickel, and M.A. Green, *Subcellular distribution of tissue radiocopper following intravenous administration of< sup> 67</sup> Cu-labeled*

Cu-PTSM. International journal of radiation applications and instrumentation. Part B. Nuclear medicine and biology, 1992. **19**(6): p. 697-701.

69. Heneweer, C., et al., *Magnitude of enhanced permeability and retention effect in tumors with different phenotypes: 89Zr-albumin as a model system.* Journal of Nuclear Medicine, 2011. **52**(4): p. 625-633.

70. Syme, A., et al., *Monte Carlo investigation of single cell beta dosimetry for intraperitoneal radionuclide therapy.* Physics in medicine and biology, 2004. **49**(10): p. 1959.

71. Hill, R.P., D.T. Marie-Egyptienne, and D.W. Hedley. *Cancer stem cells, hypoxia and metastasis*. in *Seminars in radiation oncology*. 2009: Elsevier.

72. Keith, B. and M.C. Simon, *Hypoxia-inducible factors, stem cells, and cancer.* Cell, 2007. **129**(3): p. 465-472.

73. Wright, M.H., et al., *Brca1 breast tumors contain distinct CD44+/CD24-and CD133+ cells with cancer stem cell characteristics.* Breast Cancer Res, 2008. **10**(1): p. R10.

74. Bar, E.E., et al., *Hypoxia increases the expression of stem-cell markers and promotes clonogenicity in glioblastoma neurospheres.* The American journal of pathology, 2010. **177**(3): p. 1491-1502.

APPENDIX A

RADIOLABELING PROTOCOL

Before starting:

Unfreeze ATSM-DMSO

Have (pipettes, vials, and liquids) autoclaved/sterile filtered prior to preparation.

Have balance and centrifuge ready.

Change Gloves at **<<<<<>>>>>** to minimize possibility of contamination.

1) Evaluate activity of the Cu-64 vial.
2) Evaluate volume of (Cu-64, HCl) in vial.
    a. Zero balance using identical tare vial prior to arrival of active Cu-64.
    b. Handle active vial using long handled tongs to minimize dose.
    c. Spin down active vial (capped) briefly in centrifuge to collect liquid at the bottom.
    d. Measure mass of active vial on balance.
    e. Assume density of HCl Cu-64 to be the same as water (1g/mL). Calculate the volume inside the vial.
3) All following procedure occur inside of hot lab hood.
4) Volume of Cu-64 solution is now known to be (A). Add equal volume (A) of 4:1:5 1M Glycine: 1N NaOH: dI H20. Now have 2A(B) volume mixture.
5) Add equal volume (B) 1 mM ATSM-DMSO (unfreeze before starting). Now have solution of 2B(C) volume.
6) Add equal volume (C) 2% Na-Ascorbate. Now have mixture of 2C(D) volume.

7) Mix by pipetting up and down gently. Wait 20 minutes. **<<<<<>>>>>>**

a. Prepare Sep-Pak by rinsing with 5 mL EtOH ➔10 mL DI water➔ 10 mL air blowout.

b. Prep 0.22 micron filter by washing with 5 mL EtOH.

i. All liquid from both washes may be disregarded/eliminated.

8) Extract full (D) volume from dish with 5 mL syringe with attached needle.

a. Cap and remove needle, discard into Rad. Waste needle bin in hood.

9) Pass Cu-ATSM through Sep-Pak and collect eluate

a. Evaluate the eluate for activity (should be few % of total activity)

<<<<<>>>>>>

10) Rinse Sep-pak with 5 mL DI water twice, collect DI eluate.

a. Check activity of DI water. Should be almost nothing. **<<<<<>>>>>>**

b. Discard into liquid waste container after activity check.

11) Attach Sep-Pak to 0.22 micron filter. Rinse Sep-Pak of Cu-ATSM using 500 uL EtOH then 4.5 mL sterile saline into designated sterile vial/dish capable of holding approx. 6 mL. All liquid must be reachable by syringe w/needle used for injection.

a. Do TLC to check Cu-64 is bound to ATSM.

i. Draw line approx. 1-2 cm above bottom of TLC plate. Dot with 2 uL of solution. Wait for solution to draw up TLC approx. 10 minutes.

ii. Cut TLC in half at distance between bottom and organic limit. Evaluate each half of TLC to determine activity and efficiency of binding.

12) Check activity of 5 mL solution in vial. Withdraw desired amount of activity for injection.

13) Express excess air in syringe.

    a. Have Kim-Wipe(s) around needle tip to collect any expressed liquid.

    b. With air expressed, cap needle.

    c. Wipe the syringe with Kim-wipe, check for activity. **<<<<<>>>>>**

    d. Check syringe activity

LIST OF ABBREVIATIONS

10B2	DNA repair wild-type CHO cell line
CHO	Chinese hamster ovary
CSU	Colorado State University
CT	computed tomography
Cu-ATSM	Cu-diacetyl-bis(N4-methylthiosemicarbazone)
DAPI	4',6-diamidino-2-phenylindole
DMSO	dimethyl sulfoxide
DNA	deoxyribose nucleic acid
DSB	double strand break
EBRT	external beam radiotherapy
EC	electron capture
FBS	fetal bovine serum
FDG	F-18 fluorodeoxyglucose
HIF-1	hypoxia-inducible factor 1
HIMAC	Heavy Ion Medical Accelerator in Chiba
IR	ionizing radiation
LET	linear energy transfer
MEM-α	minimal essential medium alpha
NHEJ	non-homologous end joining
NIRS	National Institute of Radiological Science
OER	oxygen enhancement ratio
PBS	phosphate buffered saline

PET	positron emission tomography
SOBP	spread out Bragg peak
TLC	thin layer chromatography
xrs-5	NHEJ mutant CHO cell line
Z	atomic number